universität wien

DISSERTATION

Titel der Dissertation

The nucleolar polynucleotide kinase and ATP-binding factor NOL9 is required for the integrity of the ITS2-ribosomal RNA processing complex.

Verfasserin

Sabrina Bandini

angestrebter akademischer Grad

Doctor of Philosophy (PhD)

Wien, 2013

Studienkennzahl lt. Studienblatt:	A 094 490
Dissertationsgebiet lt. Studienblatt:	Molekulare Biologie
Betreut von:	Javier Martinez, PhD

INDEX

The nucleolar polynucleotide kinase and ATP-binding factor NOL9 is required for the integrity of the ITS2-ribosomal RNA processing complex.

ABSTRACT

The ribosome is the protein factory of the cell. Composed of four highly conserved RNA molecules and a plethora of associated proteins, the ribosome organizes in a large and a small subunit that assembles on the mRNA to lead the translation of all cellular proteins. This essential process is predicted to use more than 60% of the resources of the cell and is subject to extensive quality control surveillance.

Ribosome biogenesis entails the transcription of the 47S pre-rRNA, and its conversion into 18S, 5.8S (long and short forms) and 28S mature rRNAs by removal of interveining spacers. Processing of these RNAs comprise an intrincate cascade of endo- and exonucleolytic events by already identified and still elusive enzymatic activities.

NOL9 is one of approximately 200 proteins required for the formation and functioning of the ribosome. NOL9 is a nucleolar protein classified as 5'-polynucleotide kinase based on its *in vitro* activity. Recently it was shown that its activity is required for efficient conversion of the 32S pre-rRNA into the mature 5.8S and 28S rRNAs, a process that involves the removal of the internal transcribed spacer 2 (ITS2).

This Thesis focuses on roles that NOL9 plays in the biogenesis of the 5.8S rRNA in human cells. I revealed that this pathway is only partially conserved between yeast and human and that the formation of the mature 5' end of the 5.8S rRNA is linked to the processing of a proximal cleavage site located 18-23nt upstream. NOL9 is involved in the processing at this proximal cleavage site, with a contribution that is independent of its ability to phosphorylate RNA substrates *in vitro*. In particular, I showed that the ability of NOL9 to efficiently bind ATP is rather involved in regulating the interaction with PELP1, LAS1L, WDR18, TEX10, SENP3 and IPO5/RanBP5; which together with NOL9 form the ITS2-ribosomal RNA processing complex.

The nucleolar localization of the complex is affected by the interaction with nucleophosmin (NPM1), a nucleolar chaperone involved in cell proliferation through the regulation of the tumor suppressor proteins p53 and ARF. In this Thesis, I report that the ability of NOL9 to efficiently bind ATP is involved in assuring the complex integrity and therefore the crosstalk of the NOL9-containing complex with NPM1. A defect in this interaction contributes to the activation of p53-mediated mechanism of surveillance in mouse primary cells.

This investigation led me to conclude that NOL9 should be considered as an ATP-binding factor required for the integrity of the ITS2-processing complex rather than an RNA 5'-kinase, and that the ATP-binding site of the NOL9 may function as a molecular switch to induce conformational changes necessary for promoting protein-protein interactions.

Die Integrität des ITS2-ribosomalen RNA Prozessierungskomplexes benötigt NOL9, einen nukleolären ATP-Bindungsfaktor mit Polynukleotidkinaseaktivität

ZUSAMMENFASSUNG

Das Ribosom ist die Protein-Fertigungsanlage der Zelle. Aufgebaut aus vier stark konservierten RNA-Molekülen und einer Vielzahl assoziierter Proteine gliedert sich das Ribosom in eine große, sowie eine kleine Untereinheit, welche sich auf der Oberfläche einer mRNA zusammensetzt, um die Translation zellulärer Proteine zu koordinieren. Dieser Prozess verbraucht voraussichtlich mehr als 60% der zellulären Ressourcen and steht unter einer ständigen Qualitätskontrolle.

Die Biogenese des Ribosoms umfasst die Transkription der 47S prä-rRNA und ihre Umwandlung in die funktionsfähigen 18S, 5.8S (lange und kurze Formen) und 28S rRNAs durch die Entfernung zwischenliegender Spacer. Die Prozessierung dieser RNAs umfasst eine komplexe Kaskade endo- und exonukleolytischer Events, welche sowohl von bereits identifizierten, als auch von unbekannten Enzymen katalysiert werden.

NOL9 ist eines von ungefähr 200 Proteinen, die für die Bildung und Funktion der Ribosomen benötigt werden. Aufgrund seiner Aktivität *in vitro* wurde NOL9 als nukleoläre 5'-Polynukleotidkinase klassifiziert. Kürzlich wurde gezeigt, dass seine Aktivität für eine effiziente Umwandlung der 32S prä-rRNA in funktionsfähige 5.8S und 28S rRNAs benötigt wird - ein Prozess, der die Eliminierung des internen transkribierten Spacers 2 (ITS2) beinhaltet.

Der Schwerpunkt dieser Doktorarbeit liegt auf der Charakterisierung der Funktion von NOL9 im Rahmen der Biogenese der humanen 5.8S rRNA. Ich konnte zeigen, dass dieser Biogeneseweg nur teilweise zwischen Hefe und Menschen konserviert ist und dass die Generierung des reifen 5' Endes der 5.8S rRNA mit der Prozessierung einer proximalen Schnittstelle verknüpft ist, welche etwa 18-23 Nukleotide upstream liegt. NOL9 ist in die Prozessierung dieser proximalen Schnittstelle involviert, seine Funktion hierbei ist jedoch unabhängig von der Fähigkeit, RNA substrate *in vitro* zu phosphorylieren. Im Besonderen konnte ich zeigten, dass die ATP-Bindeaktivität von NOL9 vielmehr an der Regulierung der Interaktion mit PELP1, LAS1L, WDR18, TEX10, SENP3 und IPO5/RanBP5 beteiligt ist, welche gemeinsam mit NOL9 den ITS2-ribosomalen RNA Prozessierungskomplex bilden.

Die nukleoläre Lokalisierung des Komplexes wird durch dessen Interaktion mit Nukleophosmin (NPM1) beeinflusst, einem nukleären Chaperon, das durch Regulierung der Tumorsupressoren p53 und ARF an der Zellproliferation beteiligt ist. Im Rahmen dieser Doktorarbeit zeige ich, dass die Fähigkeit von NOL9, effizient ATP zu binden, die Bildung eines intakten Komplexes und folglich eine funktionelle Interaktion der NOL9-Komplexe mit NPM1 beeinflusst. Ein Defekt dieser Interaktion trägt zur Aktivierung von p53-vermittelten Überwachungsmechansimen in primären Mauszellen bei.

Aufgrund dieser Beobachtungen bin ich der Ansicht, dass NOL9 funktionell weniger als RNA 5'-Kinase, jedoch vielmehr als ATP-Bindefaktor angesehen werden sollte, der für die Integrität ITS2-

prozessierender Komplexe benötigt wird, und dass die ATP-Bindestelle von NOL9 als molekularer Schalter für die Induktion von Konformationsänderungen fungieren könnte, welche wichtig für die Förderung von Protein-Protein Interaktionen ist.

INTRODUCTION

Ribosome biogenesis in vertebrates

Ribosome biogenesis is a tightly regulated cellular process that requires the coordinated activity of the three RNA polymerases. The 47S pre-rRNA is transcribed by the RNA Polymerase one (PolI) and processed into mature 18S, 5.8S (long and short forms) and 28S rRNAs. The fourth rRNA component, the 5S rRNA, is transcribed by the RNA Polymerase three (PolIII) and assembled together with the other rRNAs and 79 ribosomal proteins (RPs) transcribed by the RNA Polymerase two (PolII). Hundreds of auxiliary factors are then involved in the processing of ribosomal RNA precursors and the assembly and export of the small and large ribosome subunits (Venema and Tollervey, 1999 , Mullineux and Lafontaine, 2012).

The biogenesis of the ribosome is controlled by the proto-oncogene c-Myc that promotes cell growth and proliferation, inducing the activity of PolI and PolIII and the production of the ribosomal proteins (Gomez-Roman *et al*, 2003; Van Riggelen *et al*, 2010). The function of c-Myc is antagonized by the activity of the tumor-suppressor p53 that closely inspects the fidelity of this process. Upon ribosome biogenesis stress several RPs associate with HDM2, a key negative regulator of p53, leading to HDM2 inactivation and p53 stabilization (Dai and Lu, 2004; Zhu *et al*. (2009). Alternative mechanisms for p53 stabilization can be mediated directly by nucleolar-non ribosomal proteins as NPM1 and ARF (ADP-ribosylation factor), both able to disrupt HDM2-p53 binding (Kurki *et al*, 2004; Kamijo *et al*, 1998). In line with its role to antagonize c-Myc, p53 represses PolI transcription by binding the PolI initiation complex (Budde and Grummt, 1999).

Human pre-rRNA processing pathways

The pre-rRNA processing pathway is best characterized in *Saccharomyces cerevisiae*. The primary transcript is processed co-transcriptionally (Kos, 2010) and follows a 5’ to 3’ processing hierarchy where the 5’ external transcribed spacer (5’ETS) is cleaved before the processing of the internal transcribed spacer 1 (ITS1), which in turn is cleaved before the internal transcribed spacer 2 (ITS2) is processed. In contrast, pre-rRNA maturation in vertebrates is post-transcriptional and does not follow the 5’ to 3’ processing hierarchy. After an initial endonucleolytic removal of a minor part of the 5’ETS and the complete 3’ETS (Figure 2) from the primary transcript (47S), the mammalian pre-rRNA (45S) can be

processed by three simultaneous alternative pathways (Figure 2) involving a varying order of endonuclease cleavages (Figure 1) (Hadjiolova *et al*, 1994). The three major pathways differ in the position of the first processing event on the 45S pre-rRNA: in pathway A (Figure 2A) the first cleavage step is within the 5ETS, in pathway B (Figure 2B) is within the ITS1 and in pathway C (Figure 2C) is within ITS2 (Morello *et al*., 2011). Pathways A and B share the same ITS1 cleavage site (2c) thereby producing common intermediates (32S and 21S pre-rRNAs) while the pathway C uses a minor ITS1 cleavage site (2b) that leads to the production of a specific intermediate (17S pre-rRNA). The processing within the ITS1 (Figure 3) separates the pre-rRNAs of the small (18S) and the large (5.8S and 28S) ribosomal subunits. Three endonucleolytic cleavages in mammalian ITS1 have been reported: 2a, 2b and 2c – referred to as site 2 in Sloan *et al*, 2013– the last one being the initial cleavage site in ITS1. When the 2c cleavage site is used, the major 32S-2c precursor is produced and quickly processed to the 32S pre-rRNA by exonucleolytic trimming at the 5' end. The cleavage site 2a is mainly linked to the 3' end processing of the pre-18S rRNA and can be used as initial cleavage of the ITS1 upon defective or delayed processing at site 2c (Sloan *et al*, 2013). The use of site 2a leads to the production of the 36S pre-rRNA (Figure 3). The cleavage site 2b was reported in the minor processing pathway C (Morello *et al.*, 2011).

Figure 1: Schematic representation of the human pre-rRNA cleavage sites

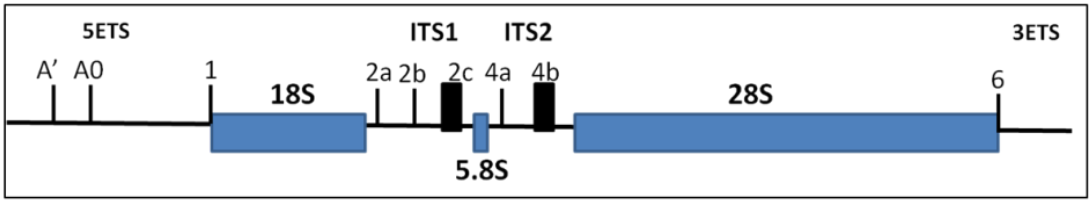

Cleavage sites in human pre-rRNA. The site 2a is located ~800nt upstream of site 2c (Sloan *et al.*, 2013), the site 2b maps ~325nt upstream of the mature 5' end of the 5.8S (Morello *et al.*, 2011). The 4a cleavage site is located ~168nt downstream of the mature 3' end of the 5.8S (Mullineux *et al.*, 2012). The cleavage sites 2c and 4b have been mapped respectively between ~207 and ~95nt upstream of the mature 5' end of the 5.8S (Sloan *et al.*, 2013) and between ~747 and ~113nt upstream of the mature 5' end of the 28S (Morello *et al.*, 2011).

Figure 2: Alternative processing pathways of the 45S pre-rRNA.

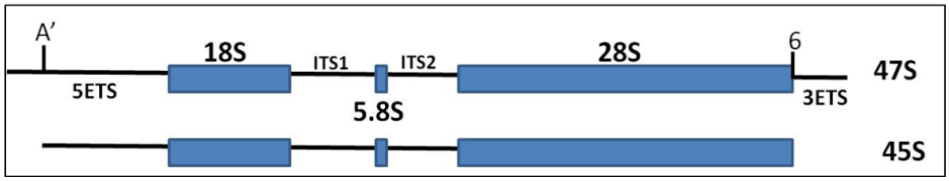

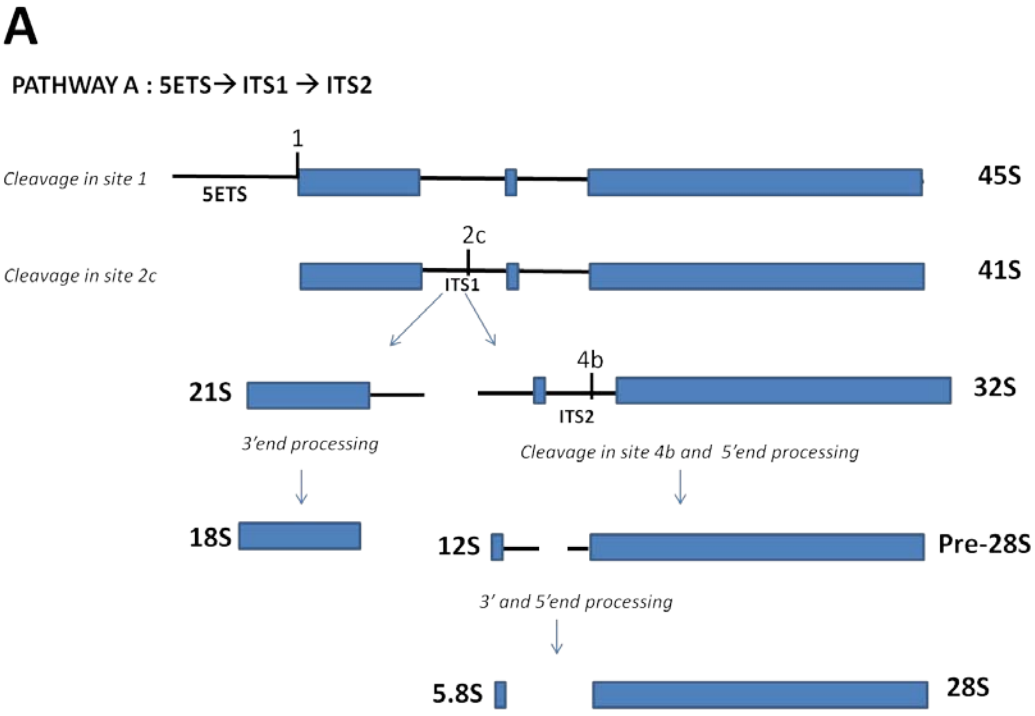

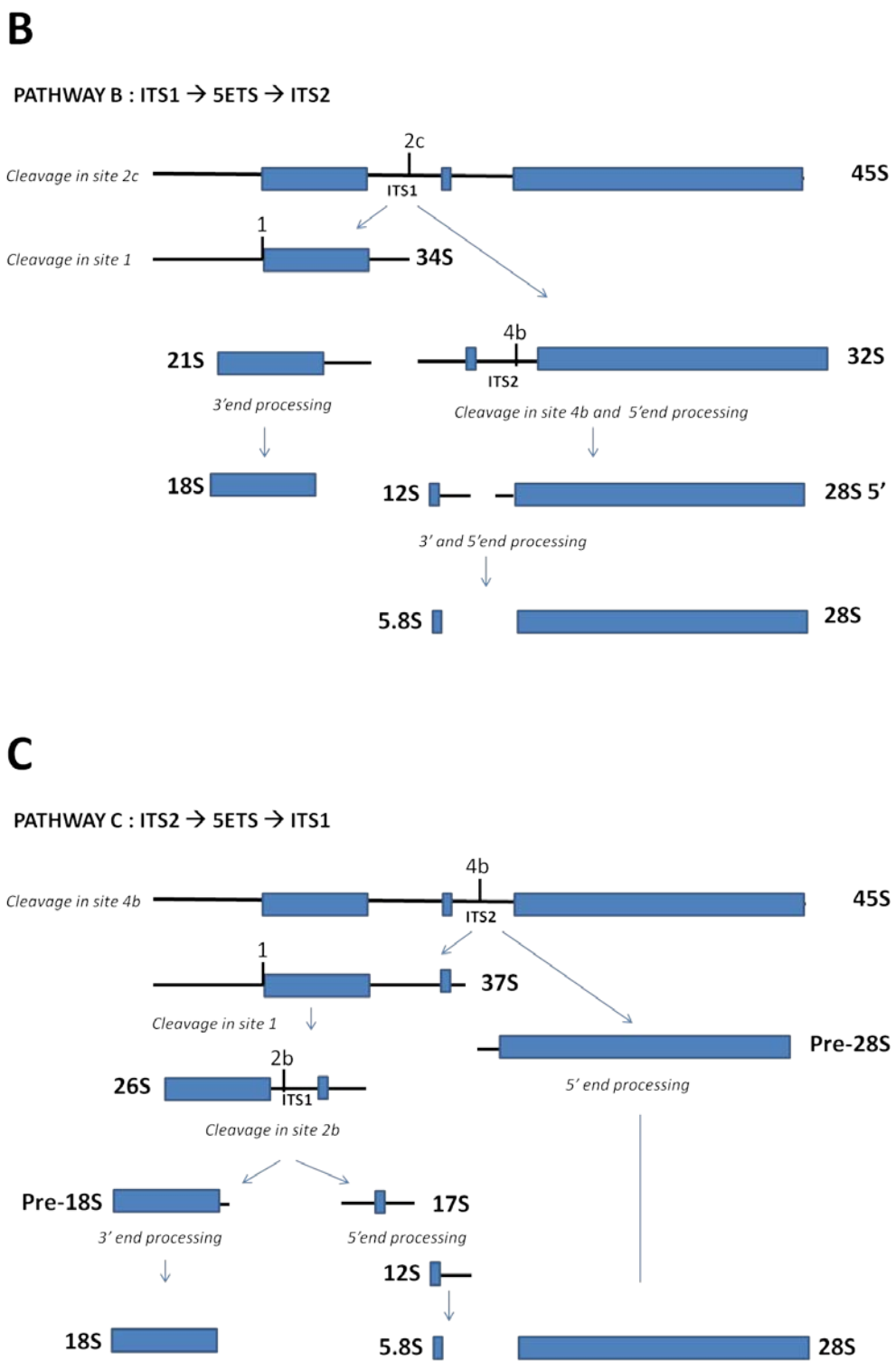

Early processing steps convert the 47S rRNA into the 45S precursor. A, B and C) Alternative processing pathways of the 45S pre-rRNA based on the paper published by Morello et al. (2011). Differences in the processing steps are described in the text.

Figure 3: Alternative processing pathways of the ITS1.

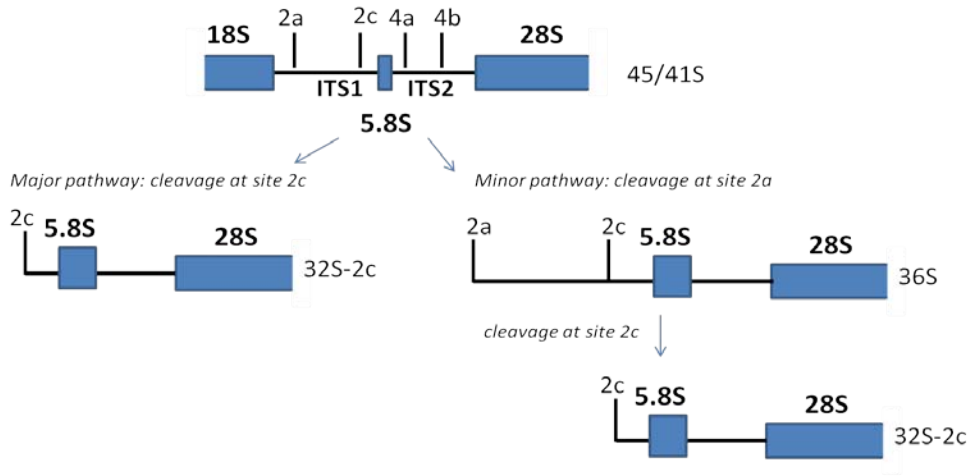

Schematic representation of the major and minor ITS1-processing pathways. The major pathway leads to the production of the 32S-2c intermediate while the minor pathway entails cleavage at site 2a prior to cleavage at site 2c, leading to the production of the 36S precursor.

Biogenesis of the 5.8S: conservation of the pathway between yeast and vertebrates.

The 5' end of the yeast 5.8S rRNA is heterogeneous. Two isoforms ($5.8S_L$ and $5.8S_S$) differing in 5-6nt at their 5' end result from the use of two alternative processing pathways (Figure 4) (Henry *et al*, 1994)**.** The $5.8S_S$ rRNA is generated by exonuclease digestion after cleavage at site A3, executed by RNase MRP. Processing from site A3 to the mature 5' end of $5.8S_S$ involves different exonucleases acting in parallel pathways: the Rat1/Rai1 heterodimer (Schmitt and Clayton, 1993; Henry *et al*, 1994) and Rrp17 (Oeffinger *et al*, 2009). In addition, the cytoplasmic exonuclease Xrn1 can degrade the fragment spanning from the A3 site to the 5'end of the mature $5.8S_S$ when Rat1/Rai1 is inactive (Henry *et al*, 1994) but it is not essential for the biogenesis of the $5.8S_S$ in normal conditions (El Hage *et al*, 2008). The presence of two different 5'→3' exonucleases (Rat1 and Rrp17) provides the cell with redundant pathways to ensure robust and efficient production of mature rRNAs. Formation of the 5' end of the less abundant $5.8S_L$ form requires neither RNase MRP, Rat1/Rai1 nor Rrp17 and it is believed to involve an unidentified endonuclease that cleaves directly the mature end of $5.8S_L$ (Faber *et al*, 2006). These two alternative pathways presumably communicate to each other to ensure a constant overall amount of 5.8S rRNA. Depletion of RNase MRP or exonucleases have a negative effect on the $5.8S_S$ rRNA but leads to a concomitant increase in the production of the long form to maintain the total amount of the 5.8S almost unchanged (Schmitt and Clayton, 1993; Henry *et al*, 1994). The mechanism behind this change in

the distribution of 5.8S rRNA forms is not clear, but there are evidences suggesting the indirect involvement of 5'→3' exonucleases (Lindahl *et al*, 2009).

The biogenesis of the 5.8S rRNA requires precise changes in the secondary structure of the rRNA. In the mature 60S ribosome subunit, both the 5' and 3' regions of the 5.8S rRNA are base paired to the 25S rRNA. However, based on secondary structure models of the ITS1 region of the 27SA3 pre-rRNA (corresponding to the 32S-2c pre-rRNA in vertebrates) it was proposed that the 5' end of the 5.8S initially base pairs to the 3' end of ITS1 (Yeh *and* Lee, 1990) forming a stable stem-loop structure, incompatible with the base pairing to the 25S rRNA, and strongly favored during the folding of the nascent transcript (Figure 5, left side). It is currently unclear whether this stem-loop has a functional role in the biogenesis of the 5.8S forms or in the coordination of the two alternative pathways, but a conformational switch of the pre-rRNA is required during the processing of the precursor of the 5.8S and 25S rRNAs. It is possible that the 5'→3' exonucleolytic trimming of the ITS1 3' fragment within the 27SA3 pre-rRNA could release the 5' end of the 5.8S rRNA, allowing the final base pairing with the 25S rRNA (Granneman *et al*, 2011) (Figure 5, right side).

Heterogeneity at the 5' end is observed for 5.8S rRNA in metazoans, plants and other eukaryotes (Henry *et al*, 1994) suggesting the use of conserved processing pathways. Most of the yeast processing factors involved in the biogenesis of the 5.8S rRNA are found in humans, but their role and requirements in the human rRNA processing pathway remain controversial. It is also unclear the structure of the 32S-2c pre-rRNA although the mature 5.8S and 28S rRNAs are known to form a binary complex with a highly conserved secondary structure in which the 5'-terminal nucleotides of the 28S rRNA and both 5' and 3' termini of 5.8S rRNAs participate to form intermolecular stems (Gutell *et al*, 1990; Michot *et al*, 1982).

Figure 4: Biogenesis of the alternative forms of 5.8S in yeast.

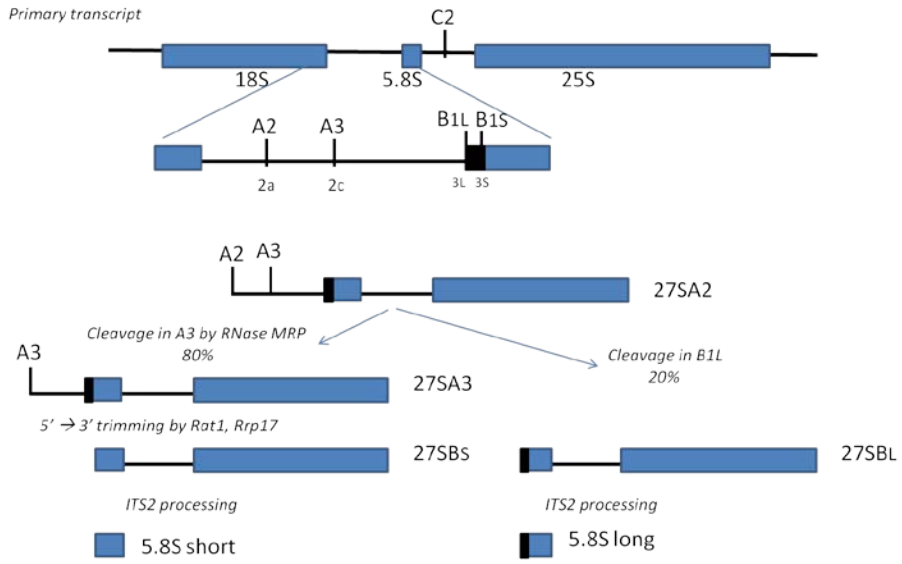

Schematic representation of the biogenesis of the $5.8S_S$ and $5.8S_L$rRNAs in yeast. The corresponding cleavage sites in mammals are indicated below the yeast names.

Figure 5: Conformational switch between the 5.8S and the 25S rRNA during rRNA processing in yeast.

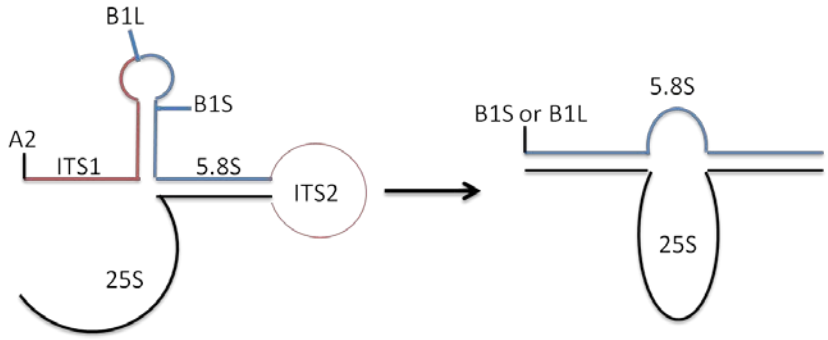

Secondary structure models of the ITS1 region of the 27SA3 pre-rRNA: the 5' end of the 5.8S initially base pairs to the ITS1 3' end (Yeh *et al*, 1990) forming a stable stem-loop structure during the folding of the nascent transcript. In the mature 60S ribosome subunit, both the 5' and 3' regions of the 5.8S rRNA are base paired to the 25S rRNA, suggesting a conformational switch of the pre-rRNA.

NOL9 and the rRNA processing

NOL9 is a nucleolar 5'-polynucleotyde kinase involved in the processing of the large subunit rRNAs. RNAi-mediated depletion of NOL9 leads to the accumulation of the 32S pre-rRNA concomitant with a drastic decrease of mature 28SrRNA levels and an altered ratio of the short and long isoforms of the 5.8S rRNA, while the maturation of the 18SrRNA is not affected. Additionally, processing of 45S and 41S precursors is slightly delayed (Heindl and Martinez, 2010).

The processing of the 32S pre-rRNA consists of two coordinated steps: the trimming at the 5' end of the 32S-2c that defines the mature 5' end of both 5.8S isoforms, and the cleavage within the ITS2 spacer that separates the precursors of the 5.8S (12S) and 28S rRNA. NOL9 is involved in the definition of the ratio between the long and short isoforms of the 5.8S (Heindl and Martinez, 2010). In yeast, the processing step responsible for the relative abundance of the two 5.8S isoforms is the maturation of the 5' end of the 27SA3 pre-rRNA (equivalent to the 32S-2c pre-rRNA in vertebrates). This processing starts with a cleavage within the ITS1 followed by alternative processing steps for the removal of the residual ITS1 fragment at the 5' end of the 27SA3 pre-rRNA (Venema and Tollervey, 1999). To gain more insight into the role of NOL9 in this context I analyzed in greater detail the cleavage steps within the ITS1 and the following 5' to 3' end exonucleolytic trimming that should produce the mature 5' end of the $5.8S_S$ in mammalian cells.

The ATP-binding and catalytic domains of NOL9 and Clp1 are conserved.

NOL9 is a nucleolar protein classified as 5'-polynucleotide kinase based on its *in vitro* activity (Heindl and Martinez, 2010)**.** NOL9 co-sediments with pre-60S particles and is required for efficient conversion of the 32S pre-rRNA into the mature 5.8S and 28S. The sequence and enzymatic activity of NOL9 is highly conserved in the yeast homolog Grc3 (Braglia *et al*, 2010; Peng *et al*, 2003), which was reported to be involved in multiple steps of ribosome biogenesis. In *Saccaromyces cerevisiae* the active kinase Grc3 contributes to the efficiency of PolI transcription termination by its direct interaction with the Rat1/Rai1 exonuclease (Braglia *et al*, 2010) while in *Saccaromyces pombe* Grc3 directly interacts with the complex required for the processing of the ITS2 fragment of the pre-rRNA and it is also involved in the formation of heterochromatin (Kitano *et al*, 2011, Castle *et al*, 2013).

The Grc3/NOL9 family is closely related to the Clp1 family of 5'-polynucleotide kinases (Weitzer and Martinez, 2007): Clp1 is involved in 3'end formation of mRNA (De Vries *et al*, 2000) and (in human, hClp1) in the splicing of tRNA precursors as a binding partner of the tRNA-splicing endonuclease (TSEN) (De Vries *et al*, 2000; Paushkin *et al*, 2004). NOL9 and Clp1 display a similar enzymatic activity *in vitro* (Heindl and Martinez, 2010) and a high sequence homology at the central catalytic domain (Figure 6). This domain contains three recognizable sequence motifs associated with nucleotide binding and hydrolysis: the P-loop/ Walker A motif (GxxxxGKS/T), the Switch I loop (DxxQ) and Switch II loop (NTxxG). The study of the crystal structure of the yeast Clp1 containing ATP bound to the P-loop and to the Switch I region (Noble *et al*.,2006) provided critical information on the role of specific conserved aminoacids in the catalytic pocket of the Clp1/NOL9 family of proteins. The lysine of the Walker A domain forms hydrogen bonds with the γ-phosphate of the ATP while the serine (or threonine) of the same loop establishes hydrogen bonds with α- and β- phosphates of the nucleotide. The serine (or threonine) of the Walker A domain is also predicted to coordinate Mg^{2+} to support the phosphoryl-transfer reaction (Ramirez *et al*., 2008). Besides, the aspartate residue of the Switch I loop is proposed to activate the 5'-OH terminus of the polynucleotide for its attack on the ATP γ-phosphate (Wang *et al*, 2002). Surprisingly the conserved aminoacid constituents of the P-loop of the yeast Clp1 are not essential for its role in mRNA 3'end formation although the same residues in hClp1 are required to sustain its ability to function in yeast tRNA splicing and *in vitro* kinase assay (Ramirez *et al*,2008). On the other hand, when the lysine and the threonine of the yeast Clp1 Walker A domain are replaced by aminoacids with opposite properties (K/E and T/W) the P-loop retains the ability to bind ATP but the protein shows a notably weaker interaction with its main protein partner Pcf11 (Ghazy *et al*, 2011) leading to the interesting conclusion that these residues are involved in ensuring the proper ATP conformation in the catalytic pocket. These observations suggest that the ATP-binding site of the Clp1/NOL9 protein family may function as a molecular switch in which the ATP binding induces conformational changes on the protein surface necessary for promoting protein-protein interactions. Differently from yeast Clp1, NOL9 shows a robust kinase activity *in vitro* (Heindl and Martinez, 2010).

In order to investigate the role of a functional ATP-binding domain of NOL9 in ribosomal RNA processing, two key residues of the P-loop, K312 and S313, were replaced with an alanine by site-specific mutagenesis. Both substitutions consistently affect the *in vitro* kinase activity in the recombinant protein NOL9-K312A and NOL9 S313A, but they show a different impact on the *in vivo* function of NOL9 in the processing of the 32S rRNA (Heindl and Martinez, 2010). One of my goals in this Doctoral Thesis was to understand the role of the ATP-binding domain of NOL9 *in vivo*, and in particular to elucidate whether the binding and hydrolysis of ATP are involved in direct phosphorylation of rRNA processing intermediates, as it is probably the case for hClp1 during tRNA splicing; or alternatively, whether the P-loop of NOL9 has *in vivo* a function that doesn't entail RNA phosphorylation.

Figure 6: Sequence motifs of putative ATP-binding and catalysis domains of NOL9 and Clp1 are highly conserved

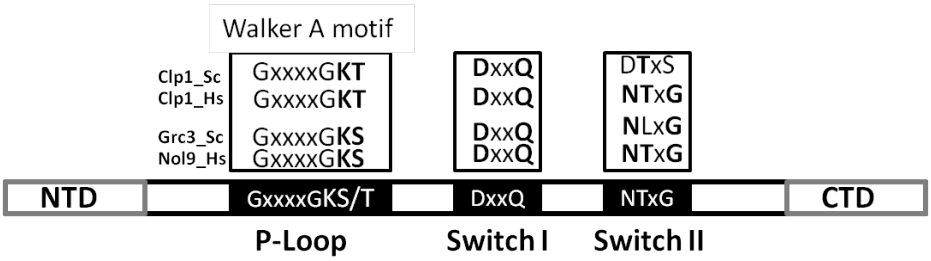

Sequence alignment of the P-loop, Switch I and II loops motifs in the central domain of Clp1 and NOL9 (Grc3) in *S.cerevisiae* and *H. sapiens*. Highly conserved residues are in bold. N-terminal and C-terminal domain are indicated (NTD, CTD).

NOL9 protein partners are involved in ribosome biogenesis.

NOL9 was reported to co-immunopurify with PELP1 and LAS1L together with WDR18, TEX10, SENP3 (Malovannaya *et al*, 2011) and IPO5/RanBP5 (Castle *et al* 2011). These proteins form a complex that co-sediments with pre-60S ribosomal particles and are required for the proper processing of 32S pre-rRNA. TEX10 and WDR18 are uncharacterized proteins that together with PELP1 form the mammalian IPI complex, described initially in yeast as required for ITS2 processing (Finkbeiner *et al*, 2011). Their interaction with LAS1L and NOL9 (in yeast Las1 and Grc3 respectively) is highly conserved (Kitano *et al*, 2011). PELP1 is the best characterized component of the NOL9 complex: apart from its involvement in ribosome biogenesis this protein is a nuclear receptor co-activator over-expressed in many cancers (Vadlamudi *et al*, 2001 and 2004); PELP1 directly binds to H3 affecting its methylation and acetylation status (Nair *et al*, 2010; Kashiwaya *et al* 2010) and its overexpression promotes G1-S progression (Balasenthil and Vadlamudi, 2003). The involvement of PELP1 in ribosome biogenesis is not limited to its

requirement for 32S pre-rRNA processing but rather extends to the regulation of the transcription of rDNA as enhancer of PolI promoter (Gonugunta *et al* 2011). The function and localization of PELP1 are finely tuned by a complex combination of post-translational modifications: its polyglutamylation influences its interaction with H3 (Kashikawa *et al*, 2010), while the phosphorylation mediated by CDKs (cycline-dependent kinases) affects PELP1 cell-cycle dependent nucleolar localization (Nair *et al*, 2010).

Nucleolar partitioning of NOL9-complex is a finely regulated process

The nucleolar localization of NOL9 and its protein partners is regulated by a combination of post-translational modifications. Both PELP1 and LAS1L were recently reported to be a target for SUMOylation. SUMO (small ubiquitin-like modifier) is covalently attached to lysine residues of target proteins and modulates the dynamics and specificity of protein-protein interactions. SUMO modification is a reversible process catalyzed by SUMO-specific proteases of the SENP family. SENP3 interaction with the NOL9-containing complex and therefore the SUMO-deconjugation of PELP1 and LAS1L determines the nucleolar partitioning of this complex as demonstrated by its delocalization from the nucleolus to the nucleoplasm upon depletion of SENP3 (Finkbeiner *et al*, 2011; Castle *et al* 2011). The nucleolar/nucleoplasmic shuttling of PELP1 and LAS1L does not affect complex composition, strongly suggesting that the assembly of the NOL9-associated complex is occurring before the association with pre-ribosomal particles (Castle *et al* 2011). The nucleolar localization of PELP1 and LAS1L (and therefore of the complex) is also affected by the interaction with NPM1 (Castle *et al* 2011), a major binding partner of SENP3 that modulates its de-SUMOylation and nucleolar localization (Yun *et al*, 2008; Haindl *et al*, 2008). NPM1 is a very abundant and highly conserved phosphoprotein that resides prevalently in the granular region of the nucleolus and shuttles between nucleolus and nucleoplasm (Borer *et al*, 1989; Yun *et al*, 2003). Its prevalent function is as molecular chaperone of both proteins and nucleic acids (Hingorani *et al*, 2000; Okuwaki *et al*, 2001) and is involved in many cellular processes such as chromatin remodeling, DNA repair, ribosome biogenesis, cell proliferation and regulation of the tumor suppressors proteins p53 and ARF. Its precise function in ribosome biogenesis is still unclear; apart from its role as a protein chaperone, NPM1 controls maturation of the 28S rRNA possibly by inducing the cleavage of the 32S precursor within the ITS2 region (Itahana *et* al, 2003; Haindle *et* al, 2008) as suggested by its intrinsic ribonuclease activity. In fact, NPM1 shows preferential cleavage of ITS2 *in vitro*, linked to the three-dimensional structure of the substrate (Savkur and Olson, 1998). Depletion of NOL9-associated complex components results in G1 arrest through stabilization of p53 (Castle *et al* 2011). The mechanism behind the crosstalk between the NOL9-containing complex, p53 and cell-cycle remains unexplored.

RESULTS

Short summary of results

The goal of this study is to understand the role of the polynucleotide-kinase NOL9 in the biogenesis of rRNA, with a special attention to the processing of the 32S-2c precursor into the 5.8S rRNA. Since this topic was almost unexplored in human this investigation starts with an accurate dissection of this step of the rRNA biogenesis. The first sections of this thesis report the study of the conservation of the biogenesis of the 5.8S rRNA between yeast and human, with a particular focus on the role of NOL9 as an active enzyme in this process. I revealed that in human cells, RNase MRP and XRN2/Rat1 cleave and trim, respectively, the ITS1 spacer very much as in yeast. Yet, in contrast to yeast, this processing step seems to be uncoupled from the biogenesis of the 5.8S rRNA. The formation of the mature 5' end of the 5.8S is surprisingly linked to the processing of a novel proximal cleavage site, located 18-23nt upstream of the 3L site, by NOL9; however it is still unclear the exact role that NOL9 plays in this step. My data indicate that the role of NOL9 in rRNA processing is independent of its shown ability to phosphorylate RNA substrates in vitro since the K312A substitution affects the kinase activity in vitro but has no impact on the ratio between the two forms of the 5.8S rRNA. On the other hand the S313 residue of the P-loop seems to be essential to guarantee the functionality of NOL9 in vivo. This first part is followed by the study of mutations that impairs the ability of NOL9 to bind ATP revealing the unexpected role of the nucleotide-binding domain of this enzyme in coordinating protein-protein interactions. I report that a functional Walker A domain, able to bind ATP, is required to allow the proper interaction of NOL9 with ITS2-processing factors. The S313A substitution particularly impairs the ability of the NOL9-containing complex to interact with NPM1, a defect that contributes to the activation of a p53-mediated mechanism of surveillance in primary cells. This part of the study contributes to a new interpretation of the already described interaction of the NOL9 complex with NPM1, in light of the strong cellular effects (p53 activation and cell cycle arrest) reported upon depletion of the components of the complex. To conclude the thesis I report the study of the ability of the complex containing an ATP-binding competent /mutant NOL9 to interact with the target rRNA (5.8S) in vivo and in vitro to further understand the contribution of NOL9 to the function of the ITS2-processing complex. My results lead to the conclusion that, in vivo, NOL9 should be considered as an ATP-binding factor required for the integrity of the ITS2- processing complex rather than an RNA 5'-kinase. Data presented in this Thesis allows me hypothesizing that the ATP-binding site of the NOL9 may function as a molecular switch to induce conformational changes necessary for promoting crucial protein-protein interactions.

The role of RNase MRP in ITS1 processing is conserved in human cells.

Depletion of RNase MRP in yeast causes a decrease in $5.8S_S$ molecules with a concomitant increase in the levels of the $5.8S_L$ form (Schmitt and Clayton, 1993). In addition, an aberrant rRNA precursor that stretches from the A2 site to the mature 3'end of the 5.8S accumulated upon depletion of RNase MRP, apparently resulting from failure to cleave within A2-B1 region that contains the MRP cleavage site A3 (Figure 7). This aberrant RNA was not seen in a wildtype strain and therefore it is not believed to be a normal rRNA precursor (Schmitt and Clayton, 1993). On the other hand, depletion of RNase MRP neither affects the amounts of 18S and 25S rRNAs nor any other precursor.

One of the main goals of this study is to elucidate the mechanism behind the biogenesis of the alternative 5.8S rRNA isoforms and the possible involvement of NOL9. To gain more insight in this process I tested the involvement of RNase MRP in the formation of the $5.8S_S$ rRNA in vertebrates. For this purpose I depleted POP1 by RNAi in HeLa cells. POP1 is a protein component of the RNase complex that is reported to be essential for the stability of the RNA catalytic subunit of MRP. The efficiency of the knockdown was confirmed by RT-qPCR on the levels of POP1 mRNA as well as directly on the level of the RNA component of MRP (Figure 8A). To study rRNA processing the RNA was extracted and separated by denaturing polyacrylamide/urea gel. A Northern Blot performed with a probe specific for the 5.8S rRNA did not show any alteration in the ratio between the two forms of the 5.8S rRNA (Figure 8 B and C). Interestingly, a longer (~650nt) processing intermediate accumulated in the POP1 knockdown sample compared to the control (Figure 8 D). The same band was detected using a probe specific for the 3'end of the ITS1, downstream of the 2c cleavage site. This fragment does not extend into the ITS2 since it was not detected using a probe directed towards the region between the cleavages sites 4a and 4b. Based on these data I conclude that the involvement of RNase MRP in the processing of the ITS1 is conserved between yeast and human. According to the size and probe specificity, we can deduce that this fragment can span from the cleavage site 2b to the cleavage site 4a and it is a normal intermediate of the ITS1 processing that accumulates probably as a consequence of a defective cleavage at site 2c – the equivalent cleavage site to the yeast A3 – known to be the target of RNase MRP. Furthermore, the failure of the ITS2-specific probe in detecting the fragment and its length suggests that this processing intermediate might extend to the 4a cleavage site, indicating a delayed processing at the 3' end of the 5.8S. It is interesting to note that the ratio of the 5.8S long and short forms is not altered although the processing at the ITS1 site 2c results affected. These evidences suggest that in human rRNA processing, the cleavage site that provides the entry point for the biogenesis of the 5' end of $5.8S_s$ might be a different one. This crucial point will be discussed in greater details later in the text.

Figure 7: An aberrant fragment is produced in the absence of MRP cleavage in yeast.

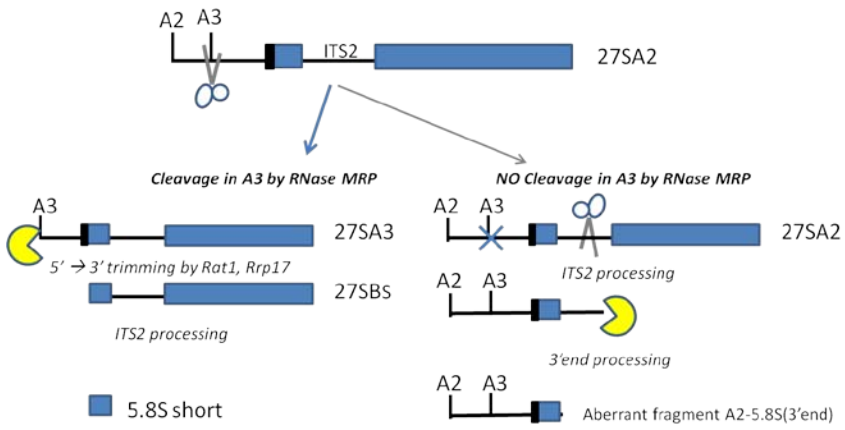

Schematic representation of the biogenesis of the 5.8S short form in the precence or absence of RNase MRP in yeast.

Figure 8: RNAi-mediated depletion of POP1 (MRP) has no effect on 5.8S rRNA biogenesis but impairs processing at site 2c.

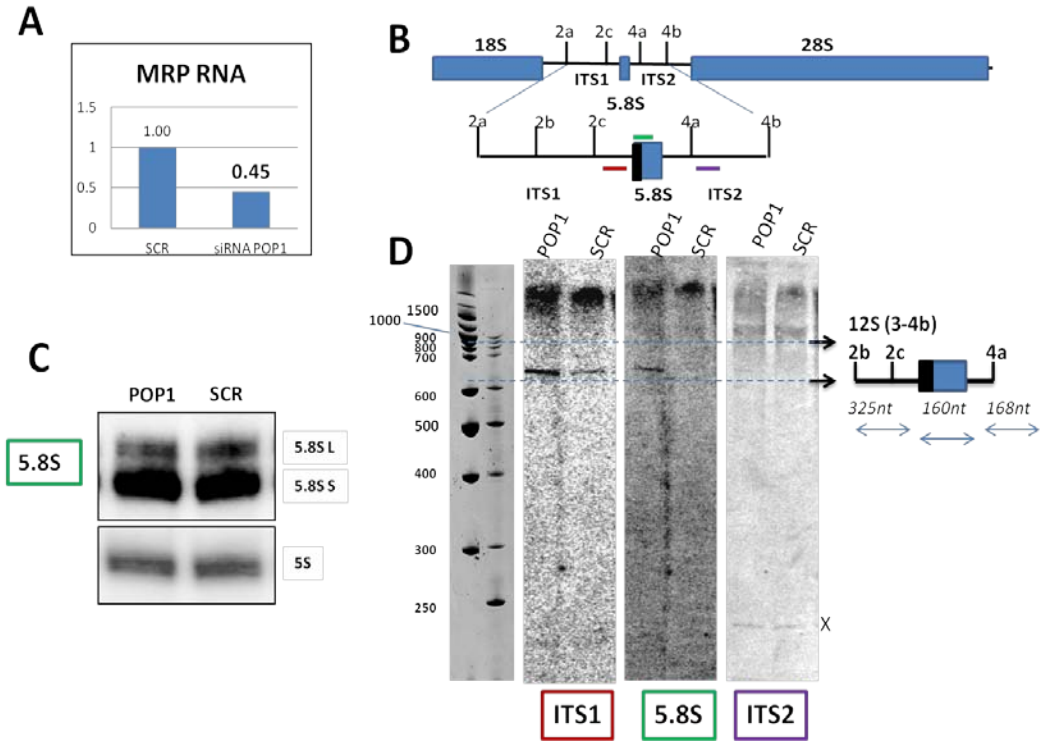

A) Analysis the MRP RNA levels analyzed by RT-qPCR (and normalized on HPRT mRNA) in siPOP1 treated cells *vs* cells transfected with scrambled (scr) siRNAs. **B)** Northern Blot probes used in C and D. **C)** Analysis of the relative abundance of 5.8S forms and normalization on 5S rRNA. **D)** Detection of the 2b-4a fragment upon POP1 knockdown compared to the control transfection (scr). Unspecific band is indicated with an X. The upper band in ITS2 probed panel is very likely to be the 12S precursor spanning from the 5' end of the 5.8S (referred to as site 3 in this figure) to 4b site (estimated size ~ 1000-1200nt).

The 5' →3' exonuclease XRN2 is involved in the trimming of ITS1 fragments in human.

Depletion of yeast Rat1 or its related protein in mammals (XRN2) and plants (AtXRN2 and AtXRN3) leads to the accumulation of 5'-unprocessed precursors of the 5.8S and 25/28S rRNA. In contrast to yeast, however, a defect in the processing of the 5' end of the 5.8S rRNA does not lead to a visible decrease in the $5.8S_S$ form, suggesting a minor role of XRN2 (and its homologs in plants) in this process and the contribution of an additional 5'→3' exonuclease (Zakrzewska-Placzek *et al*, 2010; Wang and Pestov, 2010). Furthermore, depletion of XRN2 in mammalian cells reveals pre-rRNAs derived by cleavage events that deviate from the major processing pathway (please refer to figure 3 here); a main contribution of this exonuclease in trimming suboptimal intermediates is suggested by the accumulation of the 36S pre-rRNA upon knockdown of XRN2 in mouse (Wang and Pestov, 2010). This accumulation suggests a preferential use of the minor cleavage site in ITS1 in the absence of XRN2, also reported in human (Sloan *et al*, 2013). A second 5'→3' exonuclease, Rrp17, is essential for rRNA processing in yeast and its function is very likely conserved in the mammalian NOL12 protein which belongs to an exonuclease family that differently from the Rat1/Xrn1 family can efficiently degrade substrates with 5'-OH, as well as 5'-mono-phosphates. Therefore each exonuclease is likely to have preferred substrate regions within the ITS1 (and ITS2), functioning in parallel processing pathways (Oeffinger *et al*, 2009). To verify the conservation of the function of XRN2 or NOL12 in human rRNA processing I depleted XRN2 or NOL12 in HeLa cells for 6 days (siRNA transfections repeated after 3 days, figure 9A) and analyzed the biogenesis of 5.8S rRNA by Northern Blot (figure 9B-D). Differently from what is reported in Oeffinger *et al*. (2009) and Sloan *et al*. (2013), I couldn't detect any effect in 5.8SrRNA precursors and mature levels upon depletion of NOL12 (figure 9C and D). This can be due to the long period of knockdown I used that may have allowed compensatory mechanisms to occur. However, upon depletion of XRN2, I can clearly detect the accumulation of a small fragment of ~230nt using a probe specific for the last nucleotides at the 3' end of the ITS1 (figure 9D), but it is not detectable using a probe specific for the 5.8S or ITS2. I concluded that this fragment corresponds to the product of the 2c and 3L cleavage sites – the last one being the site of the putative endonuclease generating the 5.8S long 5' end. This result confirms the conservation of the role of XRN2 in trimming the products of the ITS1 cleavage events and it is the first evidence that supports the conservation in human of the alternative 5.8S processing pathway that generates the long 5.8S rRNA by endonucleolytic cleavage at site 3L. The analysis of the long-to-short

ratio of the 5.8S forms generated a surprising result: upon depletion of XRN2 the distribution of the two isoforms of the 5.8S shifted towards the short form, which results more abundant in the knockdown than the control, concomitantly with a reduction of the abundance of the long isoform $5.8S_L$. This result diverges from the data reported in Sloan *et al*. (2013) and can probably be attributed to a delayed secondary effect due to the long knockdown period in my experiments. I can therefore conclude that the perturbation of the pathway due to the prolonged absence of XRN2 might affect the balance of the two alternative pathways generating the isoforms of the 5.8S rRNA. It is worth to note that the involvement of a 5' →3' exonuclease (Xrn1) in the up-regulation of the 5.8S long pathway in yeast was already described by Lindahl *et al* (2009): they reported that the induction of the minor pathway producing the long form of the 5.8S, detected upon RNase MRP depletion, does not occur in the absence of Xrn1.

Figure 9: RNAi-mediated depletion of XRN2 affects 5.8S rRNA biogenesis and impairs processing at site 2c.

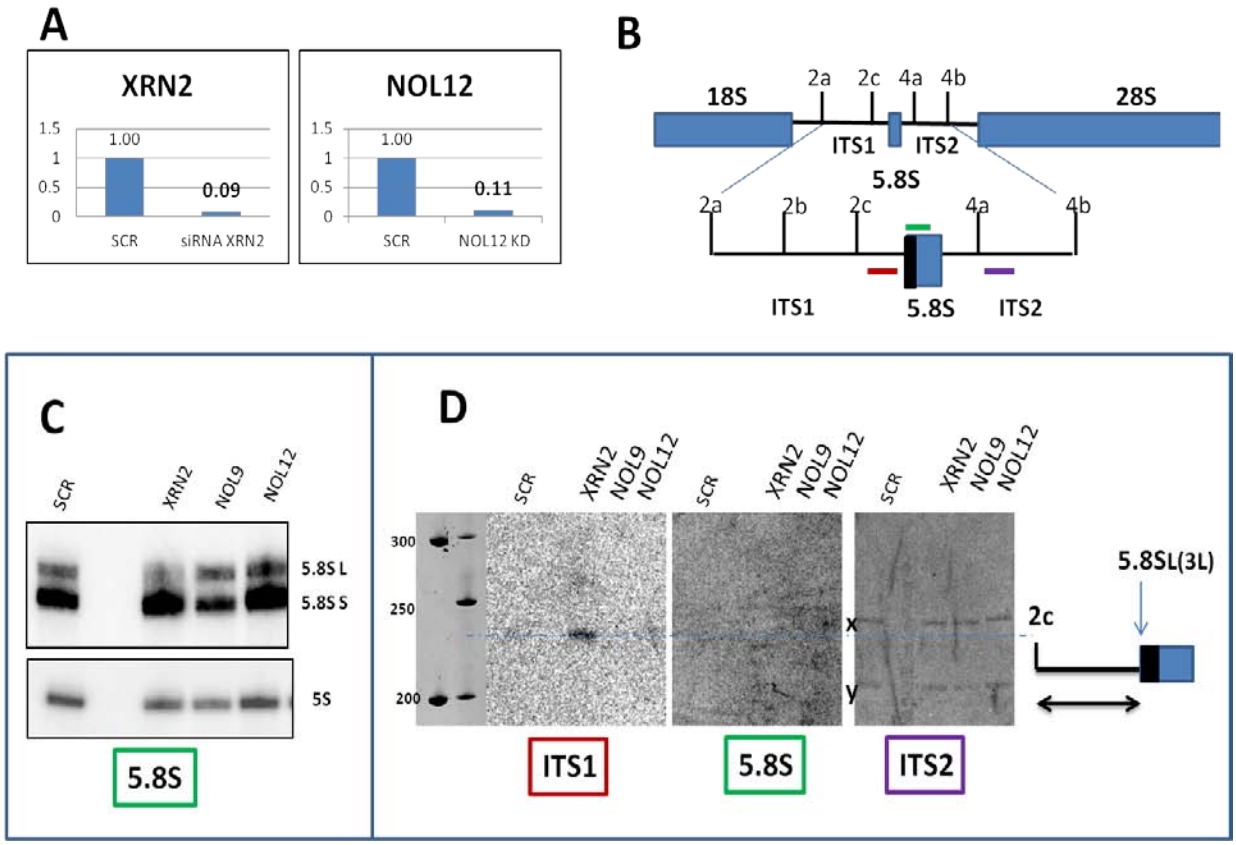

A) RT-qPCR analysis of knockdown efficiency for siXRN2 and siNOL12 (normalized on HPRT mRNA). **B)** Northern Blot probes scheme is represented. **C)** Analysis of the relative abundance of 5.8S forms and

normalization on 5S rRNA. **D)** Detection of the 2c-3L fragment upon XRN2, NOL9 and NOL12 knockdown compared to the control transfection (scr). This fragment accumulates only upon XRN2 depletion. Unspecific band is indicated with an X. The ~220nt band indicated as Y may correspond to the 4a-4b fragment.

NOL9 is required for ITS2 cleavage and optimal ITS1 processing.

NOL9 is involved in the definition of the ratio between the long and short isoforms of the 5.8S (Heindl and Martinez, 2010). To gain more insight into the role of NOL9 in this context I analyzed in greater detail the cleavage steps within the ITS1 and the following 5' to 3' end exonucleolytic trimming that should produce the mature 5' end of the $5.8S_S$. I investigated the processing of ITS1 in NOL9-depleted HeLa cells and in tamoxifen-induced, Nol9 knock-out primary MEFs (Nol9 flox/flox; CreERT2; generated by Toshikatsu Hanada). The effect of NOL9 depletion was analyzed by Northern Blot (Figure 10A) using a probe directed to the last 22nt of the ITS1 3' end. In HeLa cells this probe allow the detection of the 32S-2c precursor (not the 32S pre-rRNA) in control and in knockdown cells, showing the accumulation of this intermediate as well as the 41S and the 45/47S upon NOL9 depletion (Figure 10B). The accumulation of the 32S pre-rRNA upon NOL9 knockdown was already described in Heindl and Martinez (2010) using a probe specific for the 5.8S; due to the small difference (~200nt) between the 32S and its precursor 32S-2c it was not possible to attribute that accumulation to only one of the two intermediates. With the same probe it is also possible to detect the 36S pre-rRNA, product of the minor ITS1 processing pathway that involves the cleavage site 2a prior to the cleavage site 2c. This intermediate accumulates upon knockdown of NOL9 as well as the 32S-2c (Figure 10B right panel). The same analysis was performed in primary MEFs cells with a specific probe recognizing the same region in the 3'end ITS1. In this context this probe only allows the detection of the 36S pre-rRNA, which accumulates in the knock-out sample. To study the effect of Nol9 knock-out on 32S levels we used a probe specific for the 5.8S (Figure 10A). This analysis showed the accumulation of the 32S pre-rRNA in the knock-out sample, while it was almost undetectable in the control (Figure 10B). Based on these data I can conclude that the trimming at the 5' end of the 32S-2c occurs efficiently in the absence of Nol9 in primary mouse cells although the accumulation of the 36S pre-rRNA suggests an inefficient ITS1 processing that activates the minor pathway (cleavage at site 2a prior to site 2c). If the accumulation of 36S and 32S-2c species suggests suboptimal ITS1 processing, the accumulation of the 32S species indicates a clear impairment of the ITS2 cleavage steps. This may explain the absence of the 2b-4a processing intermediate upon NOL9 knockdown (Figure 10C). A further evidence of the negative effect of the depletion of NOL9 on ITS2 processing is suggested by the absence of the pathway C processing intermediate 17S (stretching from site 2b to site 4b) in Nol9-knock out primary MEFs (discussed later in Figure 14).

Figure 10: RNAi-mediated depletion of NOL9 impairs the processing of ITS1 and ITS2.

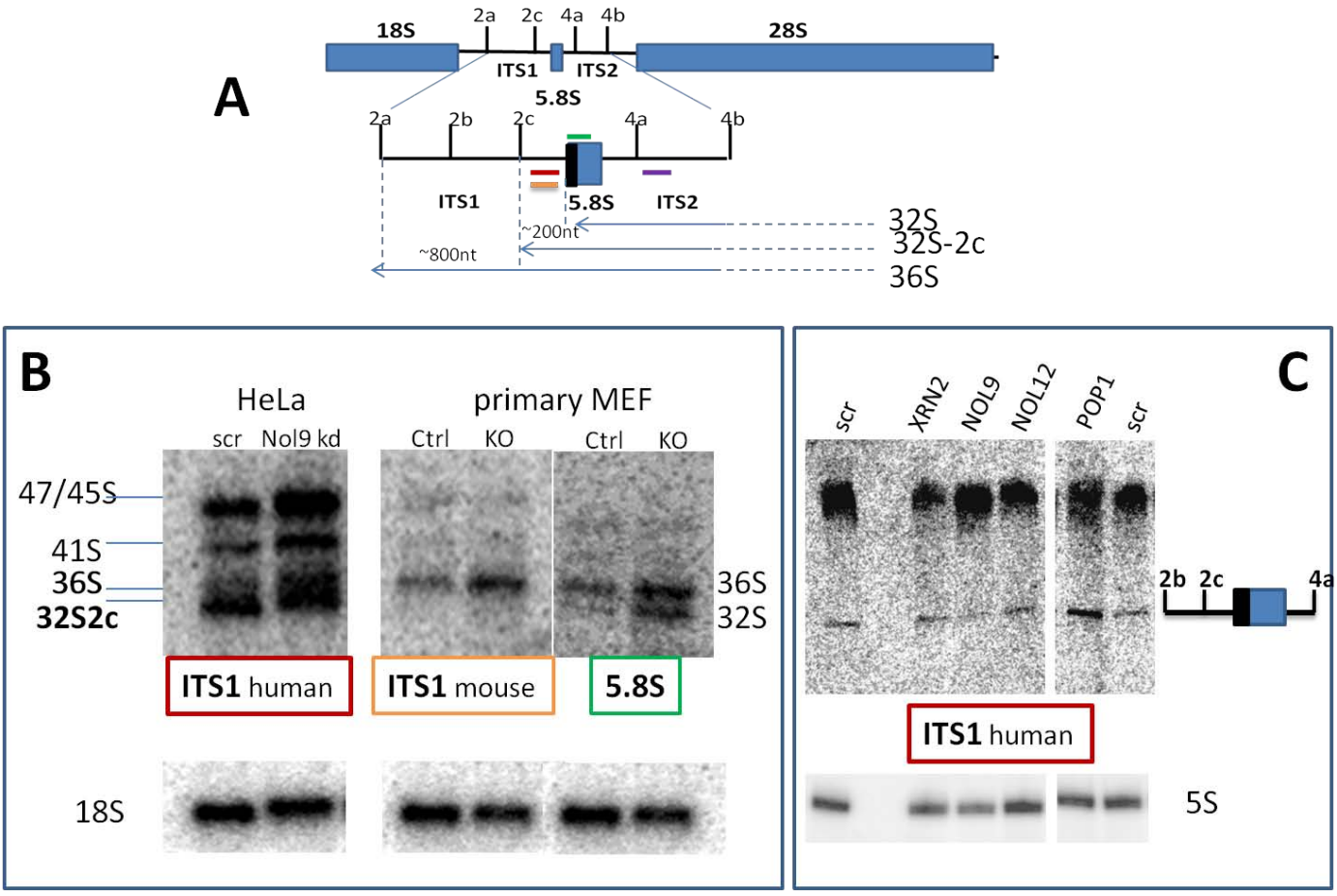

A) Northern Blot probes scheme is represented. The 5.8S probe is interspecies while two species-specific ITS1 3' end probes were used. **B)** 32S-2c specific intermediate can be detected only in HeLa cells. **C)** ITS2 processing impairment upon NOL9 knockdown can be deduced by the absence of the 2b-4a fragment.

Defective biogenesis of the 5.8S$_S$ rRNA in the absence of NOL9 correlates with inefficient processing of a proximal cleavage site located 18-23nt upstream site 3L.

In HeLa cells, the defective processing at site 2c in the absence of MRP does not directly correlate with the 5' end maturation of the 5.8S rRNA. Furthermore the accumulation of 32S-2c precursor detected upon NOL9 knockdown is not confirmed in the mouse model. These results suggest the existence of a processing site located proximal to the 5' end of the 5.8S that may be considered the main entry point for the 5'→3' exonucleases involved in the maturation of the 5.8S$_S$ (Figure 11A). A clear evidence of the existence of an alternative cleavage site, closer to the 5.8S, comes from primer extension experiments performed in yeast with a probe towards the 5.8S rRNA: Henry and co-workers (1994) first and Oeffinger and co-workers (2009) later, reported the existence of a clear stop of the polymerase in the assay at a site located 3' to the A3 cleavage site. This stop is detectable in Rat1/Xrn1 depleted cells as well as on Rrp17 depleted cells, but appears as a more prominent band upon depletion of all three exonucleases (Oeffinger et al., 2009). This stop corresponds to a putative endonucleolytic cleavage site in ITS1 at the base of the stem located 5' to the B1L site. The same band does not appear in *in vitro* transcribed RNA showing that it is not an arrest of the polymerase caused by a strong secondary structure (Henry *et al*, 1994). No evidences have been reported so far for the existence of this hairpin-like structure between the 3'end of the ITS1 and the 5' end of the 5.8S in mammals. To investigate the existence of an alternative proximal cleavage site between the site 2c and the site 3L in human rRNA I analyzed the region at the 5' of the 5.8S rRNA by primer extension. This is in fact a re-examination of the same experiment published by Heindl and Martinez, 2010**,** using a primer specific for the 5.8S (Figure 11B and C). The auto-radiography of the gel revealed a stop of the polymerase 18-23nt upstream of the mature 5' end of the long 5.8S. This stop, consistent of two predominant bands at a distance of 5-6nt, is very weak upon NOL9 depletion and this may correlate with reduced accumulation of the short form of the 5.8S. The modeled secondary structure of the same region suggests the formation of a hairpin in which the 3L cleavage site is included in a loop, while the 3S site is within the stem (Figure 12), reminiscent of the hairpin formed in yeast between the ITS1 3'end and the 5' end of the 5.8S rRNA. Secondary structure models of the 32S-2c will be required to support the hypothesis of the formation of this stem-loop *in vivo*. Yet, I can speculate that a proximal cleavage site, located 18-23nt upstream site 3L, is not used in the absence of NOL9, providing a possible explanation for the defective biogenesis of the 5.8S$_S$ in that sample. The detection of an additional cleavage site in that region may explain why the processing at the 5'end of the 5.8S in human is independent from the processing at site 2c. At the same time the existence of a new cleavage site raises the question of the identity of the enzymes involved in this processing, mainly the endonuclease and the exonuclease. A detailed analysis of the sequence spanning from the 2c and the new proximal cleavage site revealed a stretch of 18 guanosines (G-18) 65nt upstream the site 3L (Figure 12); this is a typical sequence element that interferes with the trimming by the exonucleases of the family Rat1/Xrn1 (like XRN2) as reported by Poole and Stevens in 1997. This observation may lead to the speculation that the inefficient processing of XRN2 downstream the site 2c would give the possibility to the elusive endonuclease of the 3L site to generate the long isoforms of the

5.8S; at the same time this pathway is in competition with the factors involved in the major processing pathway and in particular a putative endonuclease cleaving at the proximal cleavage site on the same RNA substrate processed by XRN2. In conclusion, in my model for the biogenesis of the 5.8S in mammals, the equilibrium between the major and minor pathways relies on the competition between two unknown endonucleases cleaving the 32S-2c precursor rRNA at the 3L and at the (*) sites. The stalling of the exonuclease (probably XRN2) favors cleavage at the 3L site. The trimming of the ITS1 starting from the proximal cleavage site (*) might destabilize the hairpin, disrupting the 3L cleavage site and leaning towards the formation of the major form (Figure 12).

Figure 11: The presence of NOL9 is linked to the cleavage at a proximal cleavage site (*) and to the biogenesis of the short 5.8S rRNA.

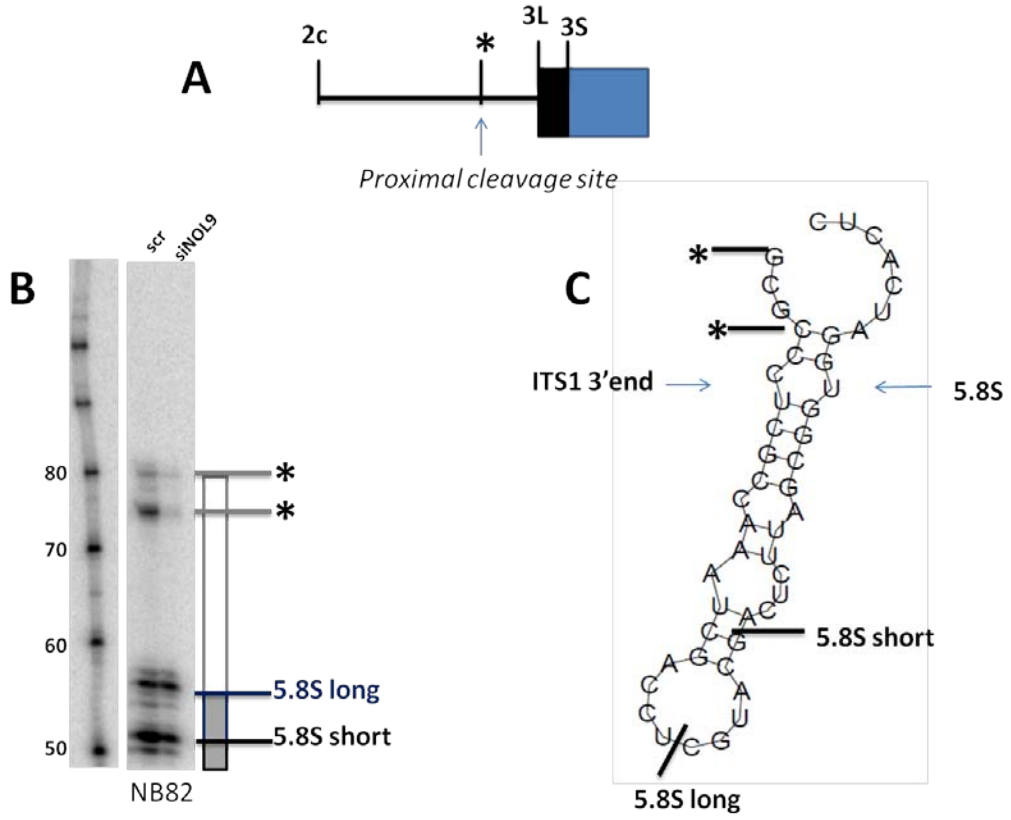

A) Schematic representation of the novel cleavage site. **B)** Primer extension was performed with probe NB82; binding 34nt downstream the 5' end of the long 5.8S form. **C)** Secondary structure prediction for the region containing the last 21nt of the ITS1 and the first 27nt of the 5.8S rRNA based on RNAFold software results ("Vienna RNA Package 2.0", Algorithms for Molecular Biology, 6:1 page(s): 26, 2011).

Figure 12: Model of the alternative pathways for the biogenesis of 5.8S rRNA in human.

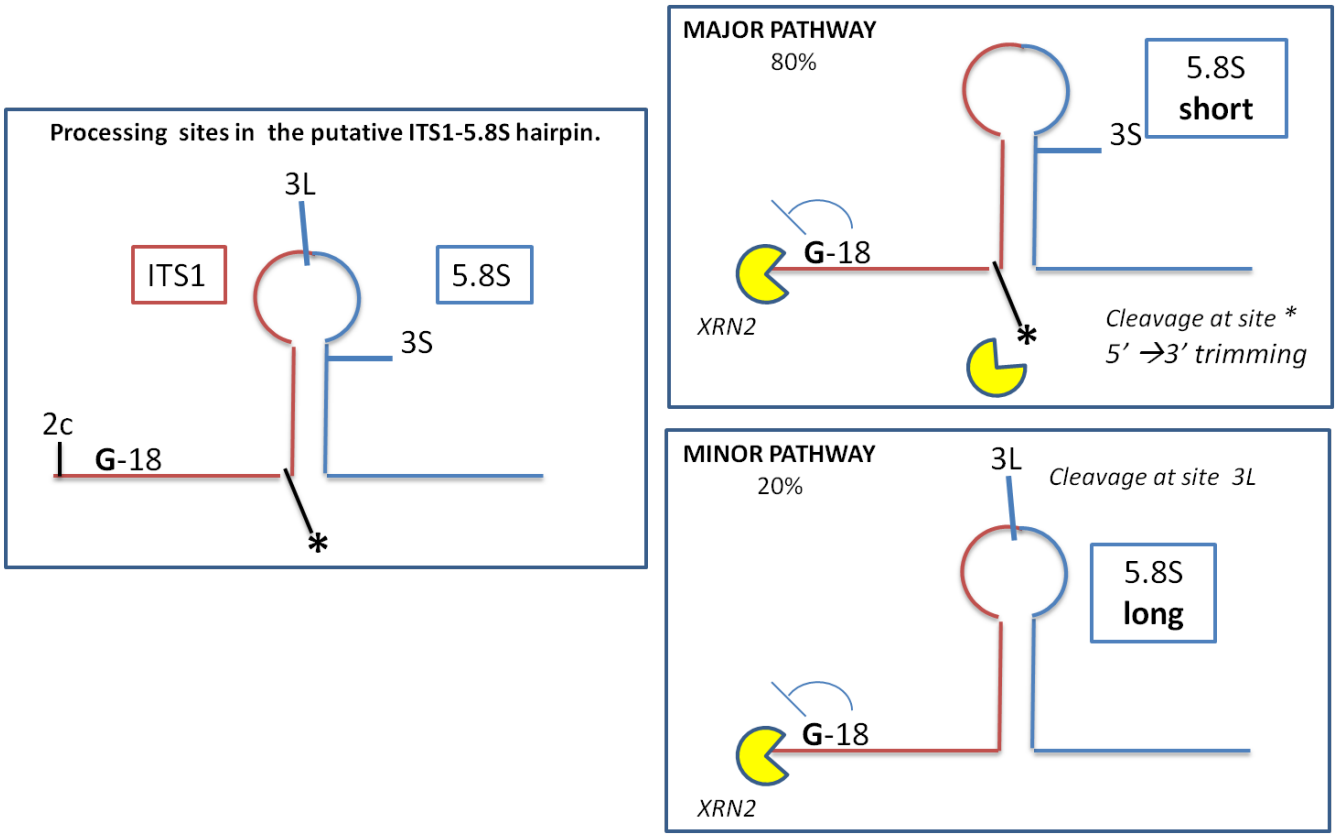

Model of the pathways for the production of the short and long forms of the 5.8S rRNA in human.

The ITS1 3' end and the 5' end of the 5.8S rRNA are indicated; this model would correspond *in vivo* to the 5' terminal region of the 32S-2c pre-rRNA. The proximal cleavage site in ITS1 is indicated as (*). 3L and 3S indicate respectively the 5' end of the long and short forms of the 5.8S rRNA. The G-rich stretch is indicated. In this model the equilibrium between the major and minor pathways is based on the competition between two unknown endonucleases cleaving the 3L and the (*) sites in the 32S-2c pre-rRNA. The stalling of the exonuclease (probably XRN2) is in favor of the 3L endonuclease. The trimming of the ITS1 starting from the proximal cleavage site (*) would destabilize the hairpin probably disrupting the 3L cleavage site, in favor of the major form production. Based on my results NOL9 is associated with the efficient production of the short form.

The function of NOL9 in 32S-2c processing is differently affected by the K312A and S313A substitutions.

In this study I aim to understand whether or not a kinase-active NOL9 is required to provide the correct ratio between the long and short forms of the 5.8S rRNA (5.8S rRNA L/S ratio). Based on previous results, we already know that the role of NOL9 is linked to the efficient production of the short form. To gain more insight into the precise function of NOL9 in this context I performed Northern Blots to monitor the levels of the two 5.8S forms in primary NOL9 knockout MEFs stably expressing the human NOL9 wildtype or the kinase-dead mutants NOL9K312A and NOL9S313A. I studied the steady-state levels of long and short 5.8S rRNAs and therefore I couldn't detect the effect of the rescue experiment 2 days after the knockout induction (Figure 13) since it is buffered by the presence of the very stable, pre-existent 5.8S rRNA. To appreciate the impact of complementing the mouse Nol9 knockout with wildtype or mutant NOL9, I analyzed the cells 5 days after depletion. The human wildtype NOL9 is able to complement the function of the mouse protein providing the cells with a normal ratio between long and short 5.8S (Figure 13, lane WT, 5d panel). Strikingly, the K312A and S313A have *in vivo* a different impact on this pathway: the K312A mutant can rescue the depletion of the mouse Nol9 leading to the production of a wildtype ratio of the long and short forms of 5.8S rRNA. In contrast, the S313A mutant shows a defective L/S ratio that results almost in an equal distribution reminiscent of the knockdown phenotype in HeLa cells (Figure 13, lane S313A, 5d panel). From these results I conclude that the kinase activity of NOL9 is not essential for determining the 5.8S rRNA L/S ratio, since the kinase-dead K312A mutant can rescue the knockout of the endogenous Nol9 in primary MEFs. Consistent results were previously reported by Heindl and Martinez (2010) for the complementation of NOL9 RNAi-depleted HeLa cells with the same wildtype and mutant constructs at the level of 32S pre-rRNA.

The processing of the 32S pre-rRNA consists in the cleavage within the ITS2 spacer that separates the precursors of the 5.8S (12S) and 28S rRNAs. Neither mutant could fully rescue the efficient 32S processing in HeLa cells but the S313A mutant showed a more severe phenotype compared to the K312A mutant, which could partially restore the processing of the 32S pre-rRNA. I further studied the *in vivo* behavior of the kinase-dead mutants and the wildtype NOL9 in knockout primary MEFs. The rescue with the S313A in primary cells lead to a strong, general block on rRNA synthesis and processing, therefore the results from this experiment could not be quantified and compared to the wildtype in terms of single intermediate processing efficiency (Figure 14). On the other hand, the steady state level of the 32S and 36S pre-rRNAs were almost the same in the wildtype and K312A mutant, indicating the ability of the kinase-dead protein to complement the role of Nol9 in ITS2 processing. Yet the efficiency of the mutant NOL9 in supporting the cleavage within the ITS2 is reduced compared to the wide-type.

A valid tool to monitor the kinetics of the processing of the ITS2 compared to the ITS1 is to analyze the processing intermediates of the pathway C where the cleavage within the ITS2 happens before the processing of the ITS1. In this Thesis I can show that the minor pathway C for the rRNA processing described in human occurs also in mouse: The detection of the 17S (2b-4b) intermediate is indicative of it, since NOL9 wildtype but not the K312A mutant can fully rescue the ITS2 processing leading to the production of the 17S pre-rRNA (Figure 14). Although the K312A mutant can process the ITS2, this

processing is slower than in the ITS1 region. Altogether these results reveal that the substitution of the K312 with an alanine does not impair the ability of NOL9 to contribute to the rRNA processing, but does affect its kinetics. This mutant can indeed produce a proper ratio of the mature rRNAs, rescuing the absence of the endogenous protein, but it is not fully efficient in this process. On the other hand, the S313 residues seem to be more essential for the *in vivo* function of NOL9 so that the substitution with the alanine has a general negative impact on ribosome biogenesis in primary cells. With these experiments I demonstrate a different behavior *in vivo* of the two Walker A mutants suggesting that the K312 and S313 residues have a different importance in guaranteeing the functionality of the protein; a difference that was not appreciated with the *in vitro* enzymatic assay.

Figure 13: The mutations K312A and S313A have a different impact on the function of Nol9 *in vivo*.

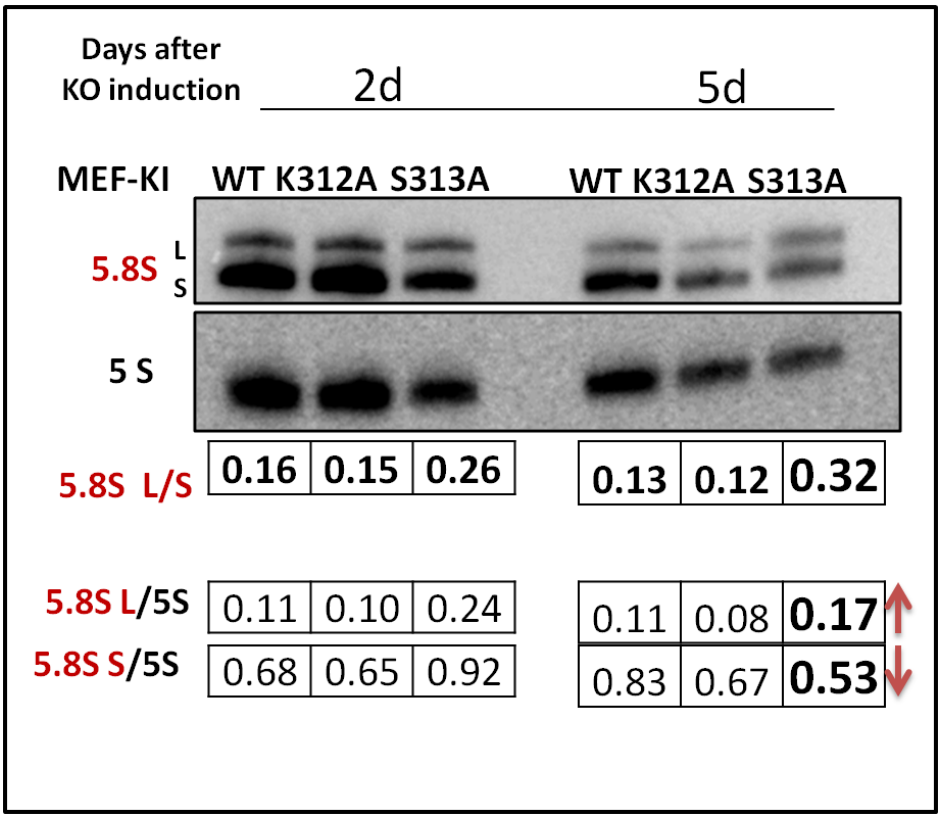

The ratio between the long and short 5.8S forms was measured after 2 and 5 days from the tamoxifen induction of the knockout (KO) in stably expressing NOL9 wildtype (WT) and mutant primary MEFs (MEF-KI). The intensity of the bands was quantified by ImageQuant software and reported as relative to the 5S rRNA abundance.

Figure 14: The wildtype and K312A NOL9 show different efficiency in the rescue of ITS2 processing.

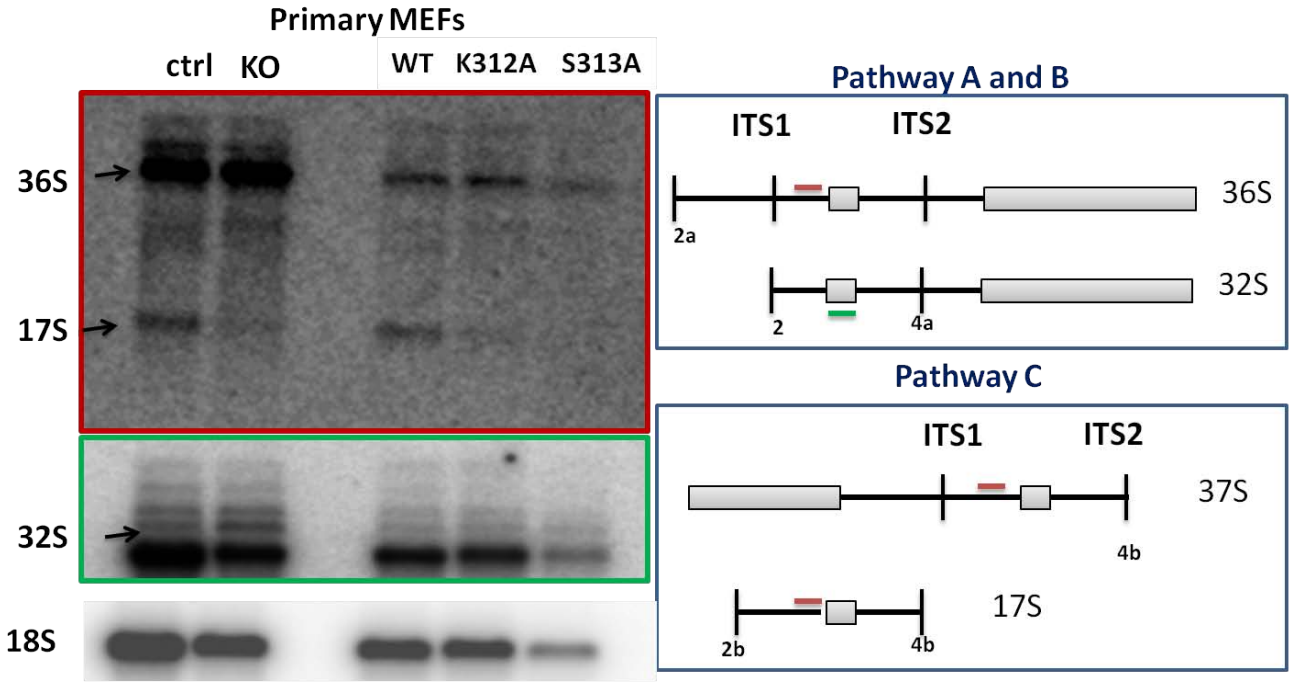

Northern Blot analysis of rRNA processing performed 2 days after induction of NOL9 knockout (KO) in control primary MEFs and in stably expressing NOL9 wildtype (WT) and mutant primary MEFs.

A functional Walker A domain of NOL9 is involved in efficient protein-protein interactions.

To further understand the role of the Walker A domain of NOL9 in ribosome biogenesis I questioned whether a well-structured ATP-binding domain is relevant for the efficient interaction of NOL9 with other proteins involved in the processing of ITS2. For this purpose I generated HEK293 cell lines stably expressing FLAG-tagged versions of wildtype (WT) NOL9, NOL9K312A and NOL9S313A, and isolated NOL9 WT and NOL9 mutant-containing complexes by FLAG-affinity purification. I revealed by mass-spectrometric analysis the co-immunopurification (co-IP) of NOL9 with PELP1, TEX10, WDR18, LAS1L and SENP3. Furthermore I revealed the association of IPO5 with NOL9 and the rest of the complex using low and high stringency purification protocols (Figure 15 A and B). I also detected the interaction of the NOL9-containing complex with NPM1. The association of NOL9 with the ITS2 processing complex and NPM1 is RNA –independent, as demonstrated by the co-immunopurification of all the components of

the complex after RNAse A/T1 treatment (Figure 15B). The MS/MS profiles of the wildtype and mutant samples were similar as well as the gel profiles of these samples (Figure 16). On the other hand, Western Blot analysis of the proteins co-purifying with NOL9 showed a clear failure of the ATP-binding mutants to interact with several protein partners (Figure 17). The interaction with PELP1 remains unaffected in mutant cells compared to wildtype, while WDR18, TEX10 and LAS1L are less efficiently co-purified with mutants NOL9. Taken together these data suggest that an ATP-binding competent NOL9 is required for the integrity of the ITS2-processing complex. Importantly, the NOL9S313A mutant shows a stronger defect in complex integrity compared to NOL9K312A, in correlation with the different impact on rRNA processing reported *in vivo*.

Figure 15: NOL9 interacts with proteins required for cleavage at ITS2.

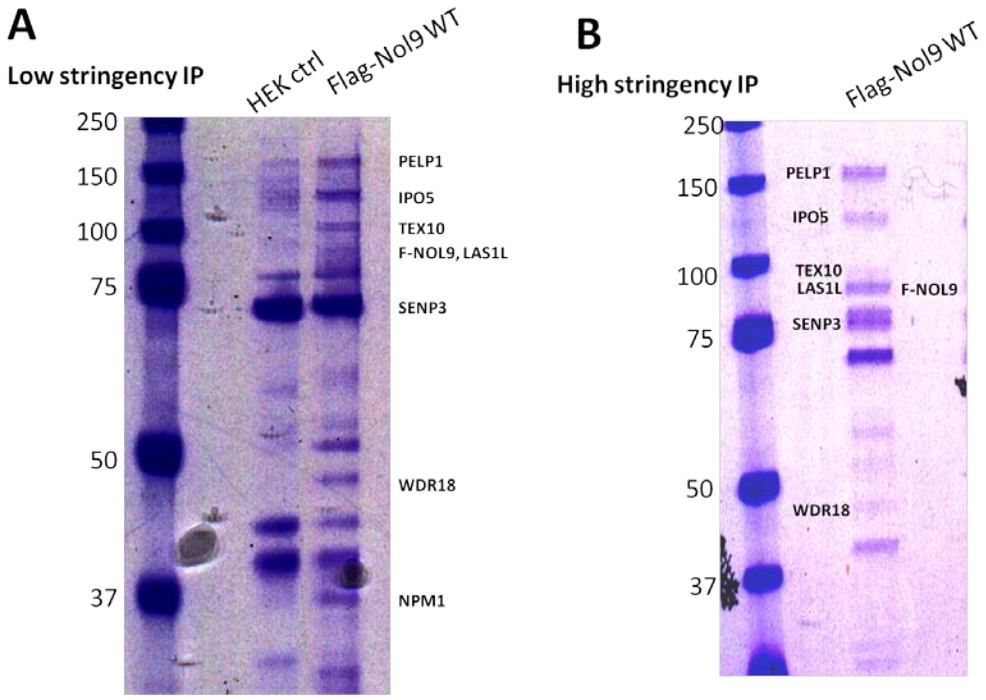

FLAG-tagged NOL9 (F-NOL9) was expressed in HEK293 cells and affinity purified using anti-FLAG M2 affinity gel. HEK293 cells were used as control (HEK ctrl). **A)** NOL9 associated proteins were separated on SDS-PAGE, stained with Coomassie Brilliant Blue (CBB) and analyzed by mass spectrometry. Identified proteins are indicated. Low stringency immunopurification (IP) was performed using 100mM NaCl. **B)** High stringency immunopurification was performed with 500mM NaCl and after RNAse A/T1 treatment. NPM1 is below the detection limit of the CBB in high stringency purification gel.

Figure 16: NOL9 kinase-dead mutants interact with the ITS2-processing complex.

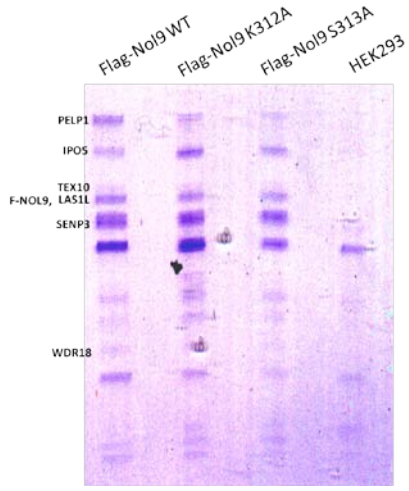

High stringency immunopurification of NOL9 WT and ATP-binding mutants was followed by SDS-PAGE, Coomassie Brilliant Blue staining and mass spectrometric analysis.

Figure 17: A functional Walker A domain in NOL9 is required for complex integrity.

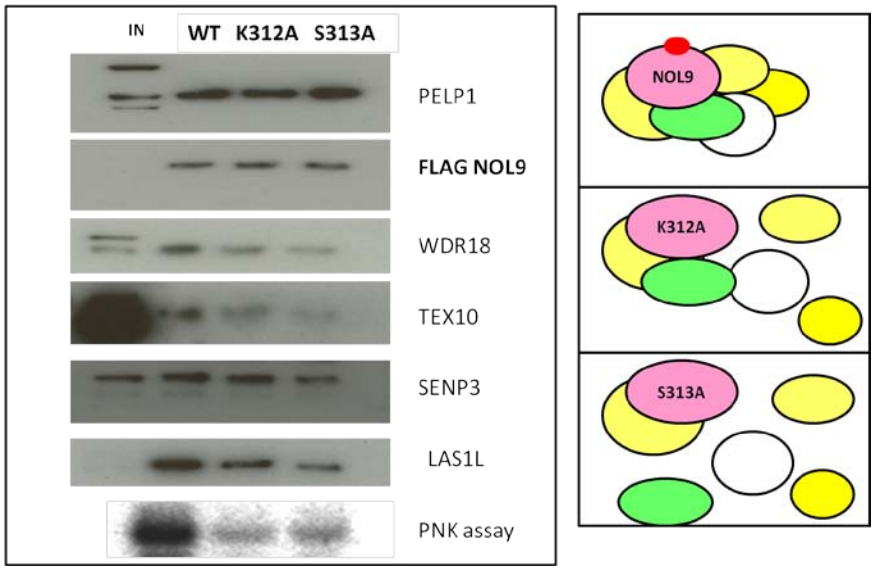

Immunoprecipitates containing FLAG-NOL9, FLAG-NOL9 K312A, FLAG-NOL9 S313A expressed in HEK293 cells were captured with anti-FLAG M2 affinity gel. The proteins eluted from the FLAG-IP were separated by SDS-PAGE and transferred to a nitrocellulose for Western blot analysis.

A functional Walker A domain is not required for NOL9 nucleolar localization.

Interestingly, only the NOL9S313A mutant associates less efficiently with SENP3 (Figure 17). The interaction between SENP3 and the NOL9-containing complex leads to SUMO-deconjugation of PELP1 and LAS1L and determines the nucleolar partitioning of the pre-formed ITS2-processing complex (Finkbeiner *et al*, 2011; Castle *et al* 2011). Therefore I wanted to investigate whether the inefficient interaction between NOL9S313A and SENP3 affects the nucleolar localization NOL9. I analyzed primary MEFs, depleted of the endogenous Nol9 and expressing either the human FLAG-NOL9 WT or mutants thereof, by immunofluorescence. This analysis revealed that the ectopically expressed FLAG-NOL9S313A localized in the nucleolus as well as the wildtype and K312A mutant, indicating that the ability of NOL9 to bind ATP is not important for sub-nuclear localization (Figure 18).

Figure 18: A functional Walker A domain is not required for NOL9 nucleolar localization.

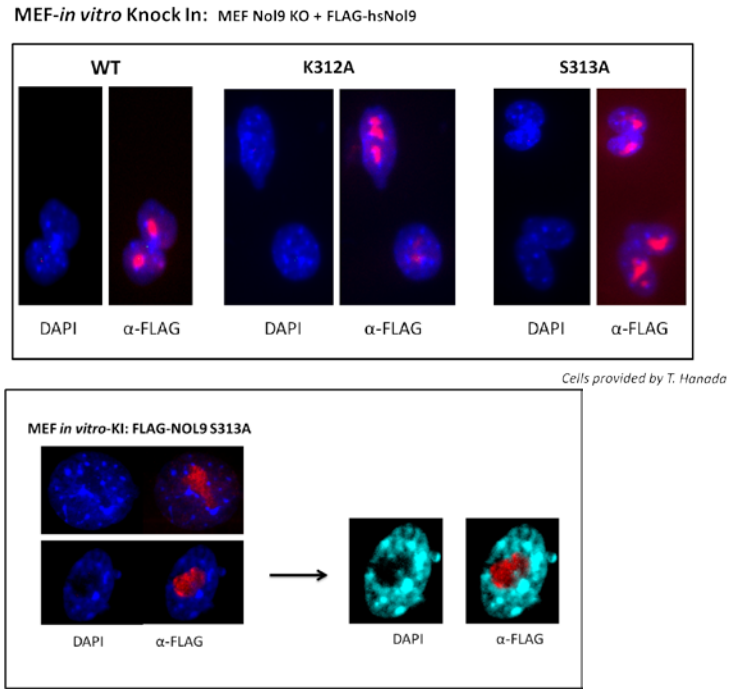

Immunofluorescence analysis of MEF cells expressing human FLAG-NOL9 wildtype and mutant: in the upper panel the nucleolar localization of NOL9 in all cell types is detected with an antibody specific for the FLAG-tag. In the lower panel is indicated the magnification of two cells of the FLAG-NOL9 S313A line. To improve the visual impact of the lower picture, the DAPI was re-colored using Image –J.

The S313A NOL9 mutation associates with defective NPM1 binding.

SENP3 has the dual function of regulating the SUMOylation status of PELP1 and LAS1L and mediate the interaction of the ITS2-processing complex with NPM1; these two events regulate the nucleolar partitioning of the complex. NPM1 is a major binding partner of SENP3, which modulates its de-SUMOylation, nucleolar localization and stability. With the aim of elucidating whether an efficient interaction of the NOL9-complex with SENP3 is required for the recruitment of NPM1 I compared the NOL9 WT and NOL9S313A FLAG-IPs for the presence of NPM1. Western Blot analysis revealed that the NOL9S313A-complex has a consistent defect in recruiting NPM1 (Figure 19), although this effect has no consequences on the nucleolar localization of NOL9. There are two possible explanations for these results: either NOL9 can localize to the nucleolus independently of other components of the complex, or the nucleolar localization of the NOL9-containing complex can occur independently of NPM1 recruitment. In support of the second hypothesis there is reported evidence that the nucleolar localization of PELP1 is mediated by its phosphorylation by CDKs (Nair *et al*, 2010), therefore I cannot exclude that the regulation of nucleolar partitioning of the ITS2-containing complex is based on multiple and redundant mechanisms. These evidences lead to the possibility that the recruitment of NPM1 to the ITS2-processing complex may have a different function, independent of the nucleolar chaperoning activity of NPM1.

Figure 1: FLAG-NOL9 S313A shows a defective interaction with NPM1.

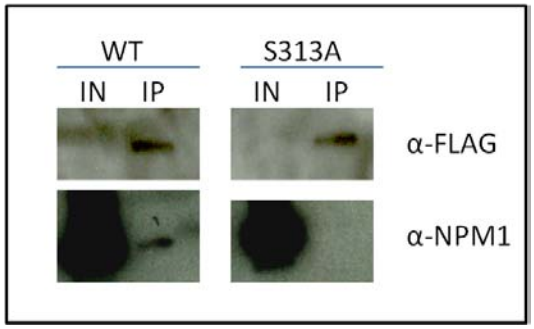

Western Blot analysis of the co-IP of NOL9 (wildtype and S313A mutant) and NPM1.

NPM1 can contribute to the crosstalk between the NOL9-containing complex, p53 and PolI transcription.

Since the defective recruitment of NPM1 has no impact on the nucleolar localization of the NOL9-containing complex I hypothesized that the lack of binding of NPM1 may affect the crosstalk between the ITS2-processing complex and p53, rather than its nucleolar localization. It has been shown that depletion of NOL9-associated complex components results in G1 arrest through stabilization of p53 (Castle *et al* 2011). I confirmed the stabilization of p53 and the subsequent induction of the expression of p21 in Nol9 knockout primary cells (Figure 20). Furthermore, the knockout of Nol9 correlates with a less efficient production of rRNA in these cells, suggesting a negative regulation of PolI transcription.

RNA PolI transcription and p53 stabilization are tightly linked: defective PolI transcription induces p53 stabilization with a consequent negative feedback on rDNA transcription. The mechanism behind the crosstalk between the NOL9-containing complex, p53 and PolI transcription is unexplored. I hypothesized that NPM1, a multifunctional protein that regulates the tumor-suppressors p53 and ARF, could be involved in this crosstalk. Upon UV-damage, or other types of damage creating transcriptional stress, NPM1 relocalizes from the nucleolus to the nucleoplasm, where by direct interaction with p53 and HDM2 (HDM2 is the ubiquitin E3 ligase responsible of p53 constitutive degradation) stabilizes p53 (Kurki *et al*, 2004). ARF protein is intrinsically unstructured and it folds upon binding to its biological substrates (Bothner *et al*, 2001). The chaperone NPM1 associates with ARF within the nucleolus and stabilizes it, increasing ARF levels in the nucleolus (Bertwistle *et al*, 2004). ARF in turns stabilizes p53 by interfering with the binding of the p53-negative regulator HDM2 (Figure 21) by sequestering HDM2 in the nucleolus (Weber *et al*, 1994; Kamijo *et al*, 1997; Sherr *et al*, 2006). Therefore an increase in nucleolar levels of free NPM1 induces ARF stabilization and the activation of p53 –mediated cell cycle arrest, including the repression of PolI transcription. The rRNA analysis of primary Nol9 knockout MEFs revealed a defect in the overall amounts of rRNA only in the NOL9S313A mutant cell line. This negative regulation of PolI transcription is linked to p21 transcriptional induction (Figure 22), suggesting p53 stabilization in that sample. This evidence may be related to the fact that only NOL9S313A shows a defective SENP3 interaction and therefore fails to recruit NPM1. Together these data support my hypothesis that the defective recruitment of NPM1 to the NOL9-containing complex can mediate the crosstalk with p53 by increasing the pool of free NPM1 in the nucleolus. The S313A mutant of NOL9 forms an aberrant ITS2-processing complex that cannot recruit NPM1; I suggest that these defects lead to inefficient processing of pre-rRNA and the stabilization of p53, which in turns has a negative feedback on PolI transcription.

Figure 20: The depletion of NOL9 leads to p53 stabilization and p21 induction.

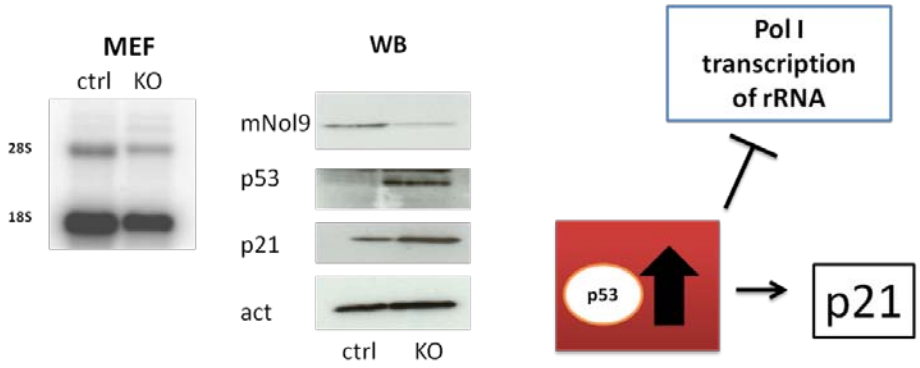

Western Blot analysis was performed using antibodies specific for the detection of p53 and p21 in mouse. Total proteins were prepared as indicated in Materials and Methods from primary MEFs control and Nol9 knock-out.

Figure 21: NPM1 can induce the stabilization of p53 via multiple pathways.

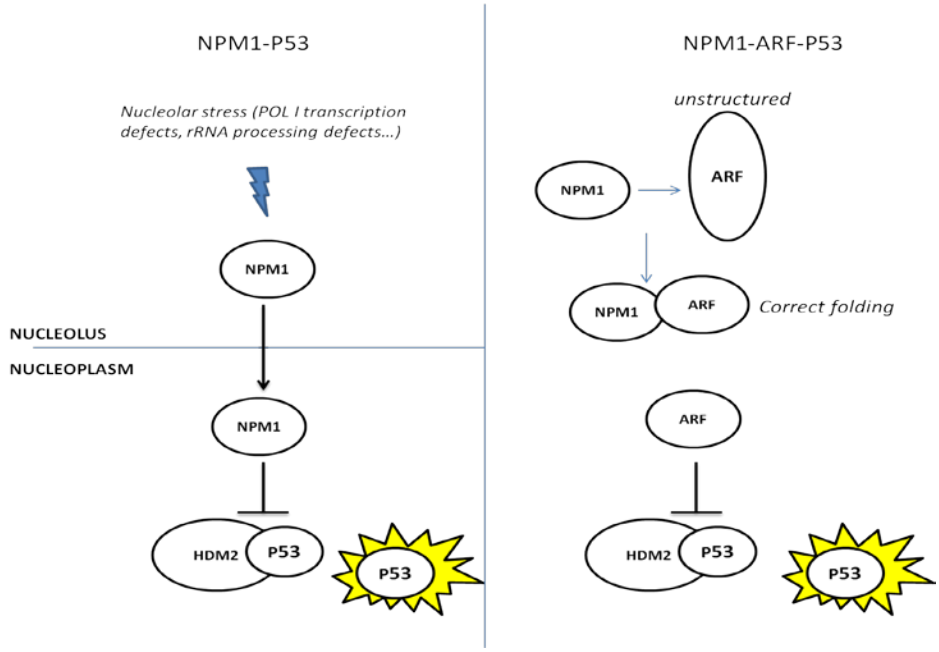

The left panel depicts the mechanism of stabilization of p53 mediated by nucleolar delocalization of NPM1: this protein is released by the nucleolus upon stress and activates p53-mediated cell cycle arrest by directly interfering with the interaction of HDM2 and p53. In the right panel is represented the stabilization of p53 mediated by the activity of ARF, upon the folding of this protein assisted by NPM1.

Figure 22: The rescue with S313A leads to p21 accumulation and inefficient Pol I transcription.

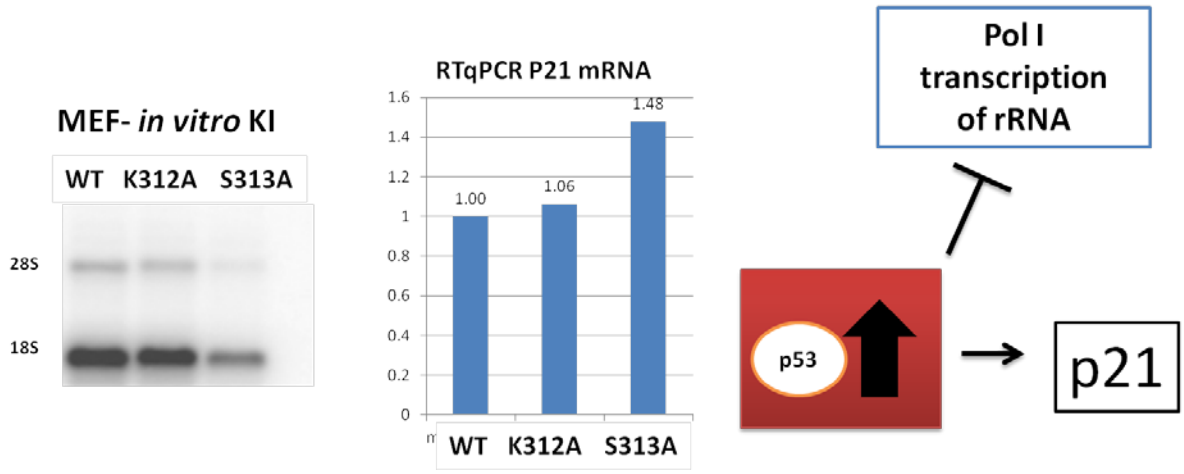

Western Blot analysis was performed using antibodies specific for the detection of p53 and p21 in mouse. Total proteins were prepared as indicated in Materials and Methods.

PolI transcription in Nol9-depleted MEF cells is mainly repressed by p53-dependent mechanisms.

NPM1 activates both p53-dependent and p53-independent pathways leading to growth arrest (Figure 23). In particular, the stabilization of ARF by NPM1 can antagonize cell proliferation by inhibiting ribosome biogenesis through p53-independent mechanisms (Sugimoto *et al*, 2003). One of these mechanisms consists in the inhibition of the nucleolar import of the PolI transcription termination factor (TTF-I). NPM1 is directly involved in the nucleolar import of TTF-I: NPM1 binds this factor probably inducing the exposure of its nucleolar localization signal (NoLS). This sequence is targeted and masked by ARF, therefore the exclusion from the nucleolus of TTF-I can be detected upon stabilization of ARF (Lessard *et al*, 2010). I already reported the stabilization of p53 in Nol9 knockout primary MEFs. Since NPM1 can induce both p53-dependent arrest of PolI initiation of transcription and p53-independent/ARF-dependent interference of PolI transcription termination, I wanted to elucidate whether the negative effect on PolI transcription can be detected in Nol9 depleted MEFs in the absence of p53. To address this question I used siRNAs to deplete Nol9 in p53-/- MEFs (Figure 24A). I isolated the nuclei from control and Nol9 knockdown-p53 knockout cells and tested the efficiency of PolI transcription by Transcriptional Run On (TRO) assay (Figure 24). This analysis revealed that in the absence of Nol9 and p53 the termination of PolI transcription is not affected. I nevertheless detected a

reduced efficiency of PolI transcription; in the absence of p53 the depletion of Nol9 had a weaker but still negative impact on PolI transcription compared to the effect described in Nol9 knockout MEFs. This suggests that the main contribution to the reduced accumulation of rRNA in Nol9 knockout primary MEFs, as well as in primary MEFs expressing the NOL9S313A mutant, can be attributed to p53-mediated mechanisms. It is therefore evident that other p53-independent mechanisms cooperate in the negative regulation of PolI transcription in association with defective formation of the ITS2-processing complex, but the data reported here allows me to exclude the ARF-dependent interference of PolI transcriptional termination as one of them.

Figure 23: ARF antagonizes the effect of NPM1 on TTF1 localization inducing POL I transcription termination.

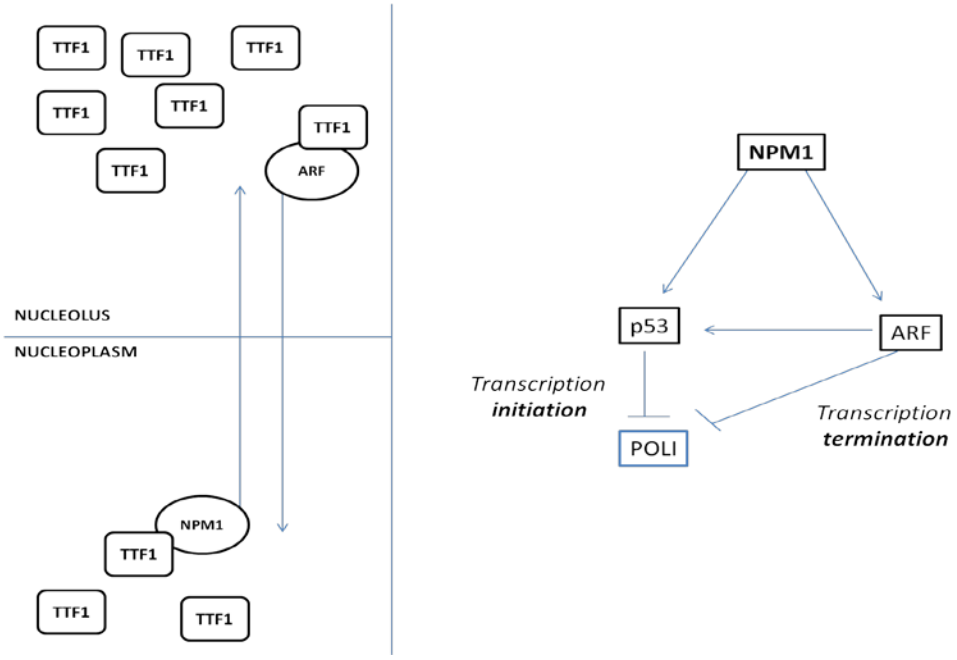

In the left panel: ARF promotes the exclusion of TTF1 from the nucleolus antagonizing the effect of NPM1, which favors the nucleolar accumulation of the transcriptional factor.

In the right panel: the repression of Pol I transcription detected upon nucleolar stress can occur at multiple levels. In the p53-mediated mechanism the transcription is affected at the initiation step, while in the ARF-dependent mechanism the termination of transcription is inhibited.

Figure 24: Depletion of Nol9 affects PolI transcription efficiency in primary MEFs in a p53-dependent manner without affecting PolI transcription termination.

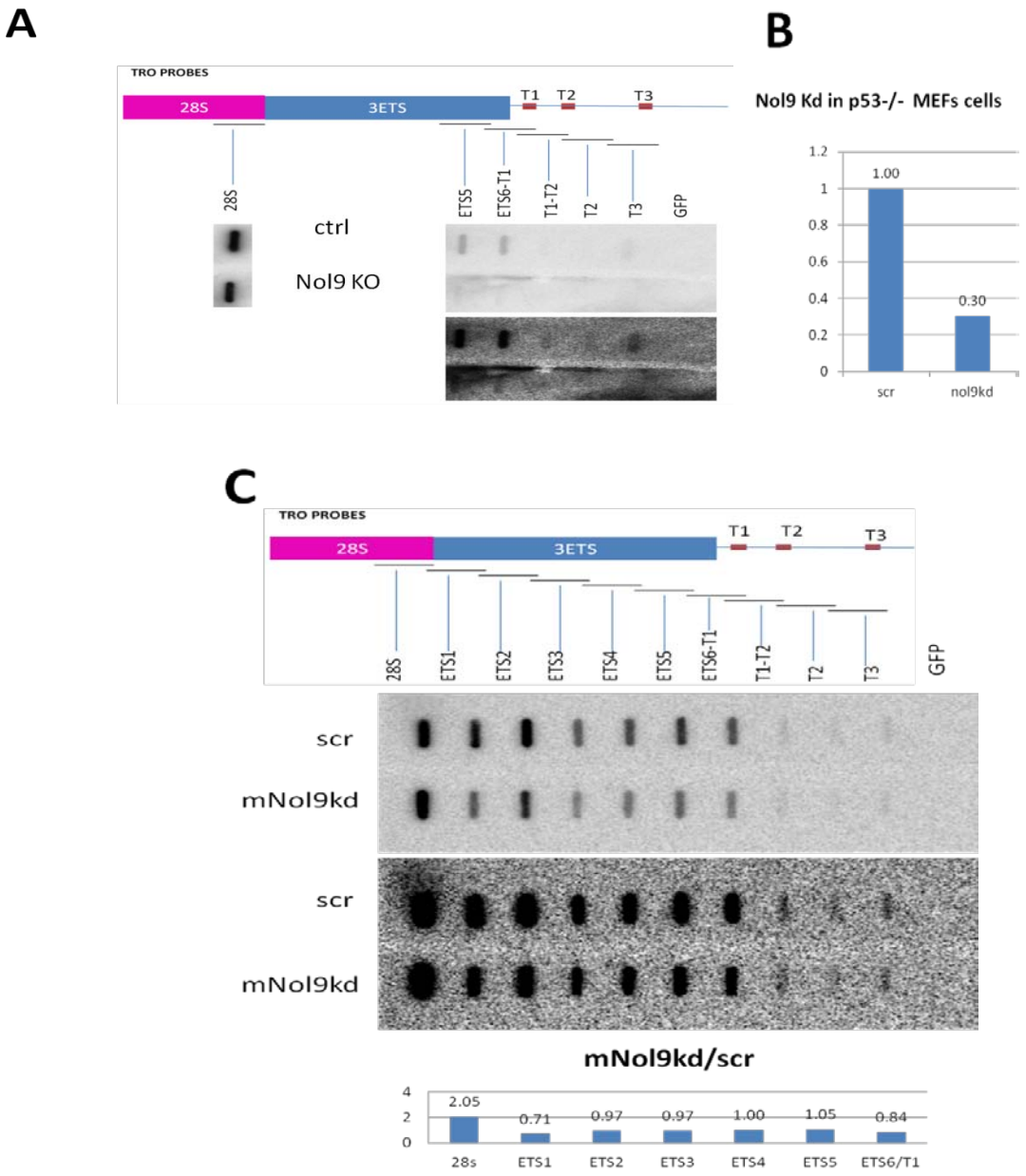

A) Nol9 knockout strongly affects PolI transcription efficiency in primary MEFs. Equal amounts of primary MEFs NOL9 flox/+; CreERT2 (ctrl) and NOL9 flox/flox CreERT2 (Nol9 KO) were treated with tamoxifen and nuclei were isolated after 72h. *In nuclei* transcription was performed at 30°C for 15 min, followed by RNA isolation. Slot Blot analysis was performed using ssDNA probes covering the termination region and the 3ETS as described in the figure. A GFP-specific probe was used as negative control. **B)** RT-qPCR analysis of Nol9 depletion in p53 knockout MEFs. Normalization of Nol9 mRNA

values was based on GAPDH levels **C)** Nol9 depletion in p53 knockout MEFs does not impairs PolI transcription termination but affects PolI transcription efficiency, although to a less extends than in primary MEFs. The quantification of band intensities was normalized on the ratio of the band ETS4 Nol9Kd (knockdown)/scr (scrambled transfection).

PELP1 destabilization can contribute to the negative regulation of PolI transcription in NOL9-depleted cells.

Although p53 seems to be the main regulator of PolI transcription in NOL9-depleted cells the transcription of rRNA in MEFs depleted of Nol9 is not as efficient as in the control. In this case I hypothesized that the interaction between NOL9 and PELP1 may have a direct effect in regulating PolI transcription efficiency independently of p53: in fact PELP1 regulates transcription of rDNA as enhancer of PolI promoter (Gonugunta *et al* 2011). To investigate whether NOL9 is important for PELP1 nucleolar functions I analyzed the stability of PELP1 upon knock-down of NOL9 and other members of the complex by Western Blot (Figure 25). The depletion of NOL9 and SENP3 as well as of TEX10 and WDR18 (already reported in Finkbeiner *et al*, 2011) affects the stability of PELP1 and this event may reduce the availability of PELP1 for binding the rDNA promoter. Furthermore PELP1 together with SENP3, TEX10 and LAS1L were reported to associate with the MLL1-WDR5 super-complex, involved in chromatin remodeling and transcriptional activation (Kashikawa *et al*, 2010; Dou *et al* 2005). To investigate whether NOL9 is also interacting with MLL1-WDR18 complex I searched for key components of the chromatin remodeling complex in the mass spectrometric profile of FLAG-NOL9 but couldn't detect any of them – MLL1, WDR5, ASH2L, RbBP5 and HCF1. I also failed in co-immunoprecipitating NOL9 with PELP1-binding target H3 (data not shown) suggesting that NOL9 might not be directly involved in chromatin remodeling. Further investigations will be required to understand whether there is a competition for the recruitment of PELP1 between the ITS2-processing complex and the chromatin remodeling super-complex and if a defective composition of the rRNA processing complex can affect the function of the MLL1-WDR5 complex. According to my preliminary data I can conclude that the destabilization of PELP1 detected upon depletion of NOL9 can contribute to the negative regulation of PolI transcription detected in Nol9 knockout primary MEFs in a mechanism that is independent on p53 stabilization.

Figure 25: NOL9 depletion affects the stability of PELP1.

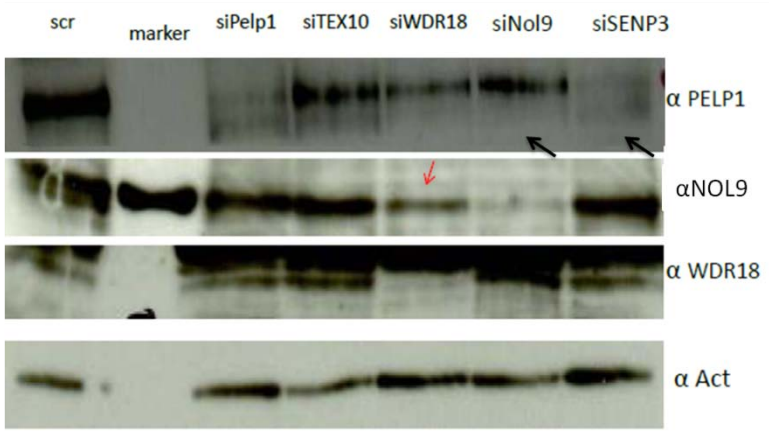

Western Blot analysis of NOL9 protein partners upon RNA interference.

NOL9-containing complex binds 5.8S rRNA *in vivo* and *in vitro.*

Data in this Thesis so far demonstrates the requirement of a functional ATP-binding domain in NOL9 to maintain the integrity of the ITS2-processing complex. A defective complex triggers the activation of a complex network of signals involving NPM1 and p53. It is still unclear whether the interaction of the ITS2- processing complex and NPM1 has a main function in the processing of ITS2. In fact NPM1 was reported to bind the ITS2 region directly and therefore to play an essential role in the cleavage of this region (Itahana *et* al, 2003; Haindle *et* al, 2008; Savkur and Olson, 1998). Another subunit of the NOL9-complex, PELP1, was reported to bind RNA, but its ability to bind rRNA was never explored (Nair *et al*, 2006). I decided to investigate whether the components of the ITS2-processing complex can bind precursor rRNAs and if that binding can occur independently from the interaction with NPM1. To address this question we explored the binding of the FLAG-NOL9 WT-complex to RNA *in vivo* by PAR-CLIP (Photo-activatable Ribonucleoside Cross-Link and Immuno-Precipitation) (Hafner *et al*, 2010). HEK293 cells, stably expressing FLAG-NOL9 wildtype, were incubated for 14 hours with the photo-activatable ribonucleoside 4-thiouridine. Cells were irradiated with UV light (365 nm) and then collected to perform FLAG-affinity purification. The RNA-protein complexes were separated by SDS-PAGE and the main bands on the gel revealed that three proteins co-purifing with FLAG-NOL9 can bind RNA *in vivo*; one band above 150 kDa, a second of a size above 75 kDa and a smaller protein below 50 kDa. These sizes could correspond to PELP1 (170-180 kDa), NOL9 (79 kDa) or LAS1L (83 kDa) and WDR18 (49 kDa) respectively. The sequencing analysis revealed an enrichment of rRNA sequences for the RNA-protein complex of ~ 75-80 kDa. The rRNA sequence most enriched in this band corresponded to the 5' end of the 5.8S rRNA (Figure 26) confirming the relevance of the ITS2-processing complex in the biogenesis of

the 5.8S rRNA. These results suggest that the RNA binding function of the ITS2-processing complex relies on multiple proteins (most likely NOL9 or LAS1L and WDR18). To further analyze the binding of the NOL9-containing complex to the 5.8s rRNA I performed an *in vitro* RNA UV-crosslinking assay followed by RNase T1 treatment, using affinity purified FLAG-NOL9 wildtype or the mutants FLAG-NOL9 S313A and FLAG-NOL9 K312A. I analyzed their ability to bind RNA *in vitro* using a RNA Pol T7 transcribed template covering the full sequence of the human 5.8S rRNA. The results of this *in vitro* RNA-crosslinking assay revealed that the sequence (or structure) of the 5.8S rRNA can be bound by two proteins that co-purify with the FLAG-NOL9 (Figure 27), one protein of more than 150 kDa (probably PELP1) and a second protein of ~80 kDa (NOL9 or LAS1L), confirming the results described for the *in vivo* analysis. No bands of 50 kDa were detected with this assay. Interestingly the binding of these proteins to the 5.8S rRNA is independent of the ability of NOL9 to efficiently bind ATP, as shown in the FLAG-NOL9 mutant samples. We can therefore conclude that the aberrant ITS2-processing complexes, containing mutant versions of NOL9, can not only still localize in the nucleolus but can also bind the target RNA, independently from the interaction with NPM1. Based on these results I speculate that the ITS2-processing complex and NPM1 need to interact on the ITS2 rRNA to promote the cleavage that initiate the processing of the 32S. The ability of NOL9 to efficiently bind ATP in the Walker A domain is essential to ensure a functional complex composition that will allow to coordinate the binding of the ITS2-processing complex on the rRNA with the interaction with NPM1. The K312A mutation may affect only marginally the role of the Walker A domain of NOL9 to bind ATP, therefore the aberrant complex integrity that derives from this mutation affects the kinetics of rRNA processing without radically arresting it. On the other hand the S313A mutation may disrupt more severely the ability of NOL9 to efficiently bind and coordinate ATP. This leads to the inability of the NOL9 containing complex to tightly interact with SENP3. This aberrant complex cannot recruit NPM1 with drastic consequences at the level of rRNA processing that lead to the activation of p53-mediated arrest of the cell cycle (Figure 28).

Figure 26: A direct evidence of the binding of NOL9-containing complex to the 5'end of the 32S rRNA

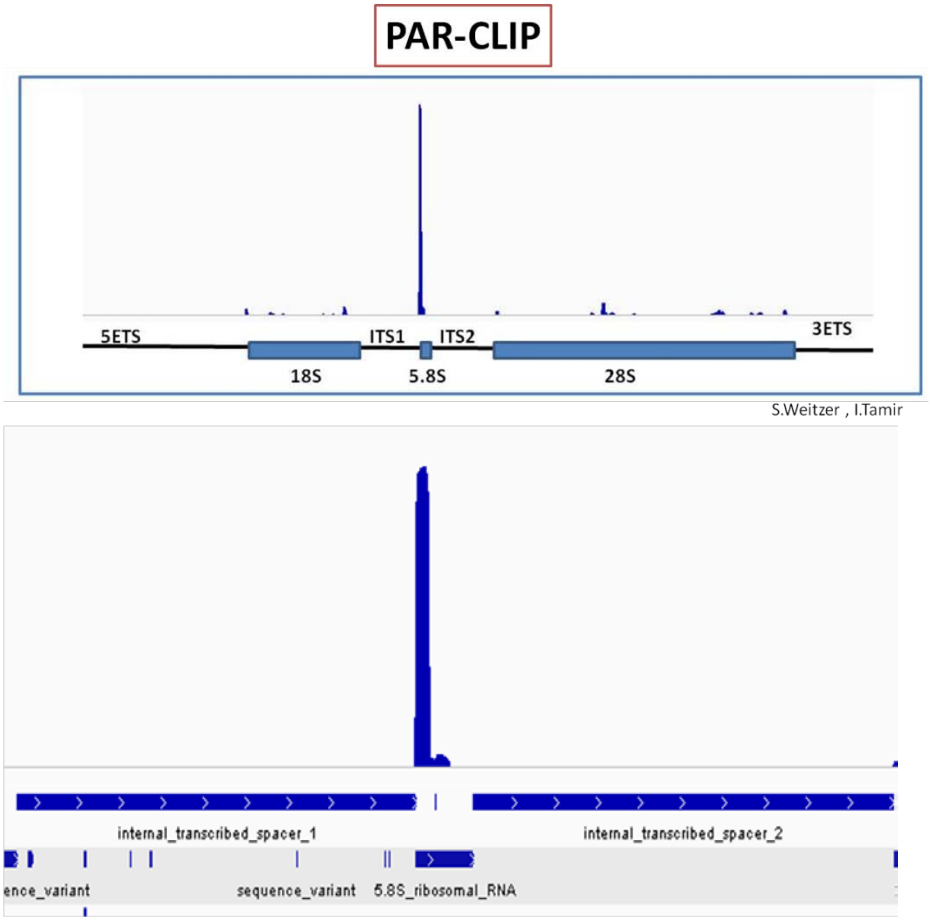

The upper panel shows a schematic representation of the distribution of sequences along the rRNA gene enriched in the FLAG-NOL9 IP obtained in the PAR-CLIP experiment. The main peak aligns with the 5'end of the 5.8S rRNA. The lower panel shows the same picture with higher resolution.

Figure 27: ATP-binding ability of NOL9 is not required for the ITS2-processing complex to bind 5.8S rRNA

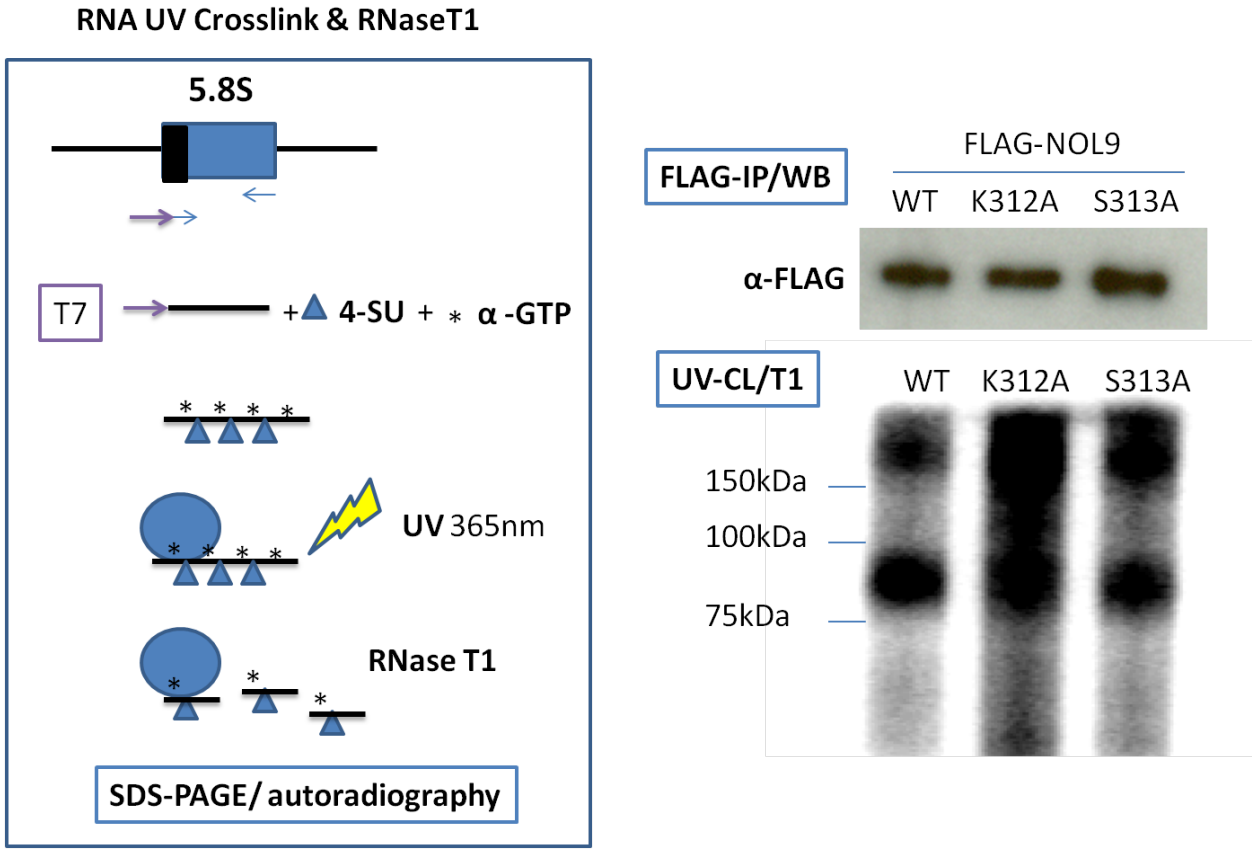

The left panel represents a schematic overview of the experimental procedure. Normalized amounts of wildtype and mutants FLAG-NOL9 IPs were used for the assay. The results indicate two main bands in the gel, one above 150 kDa, and a second of a size above 75 kDa.

Figure 28: The final model.

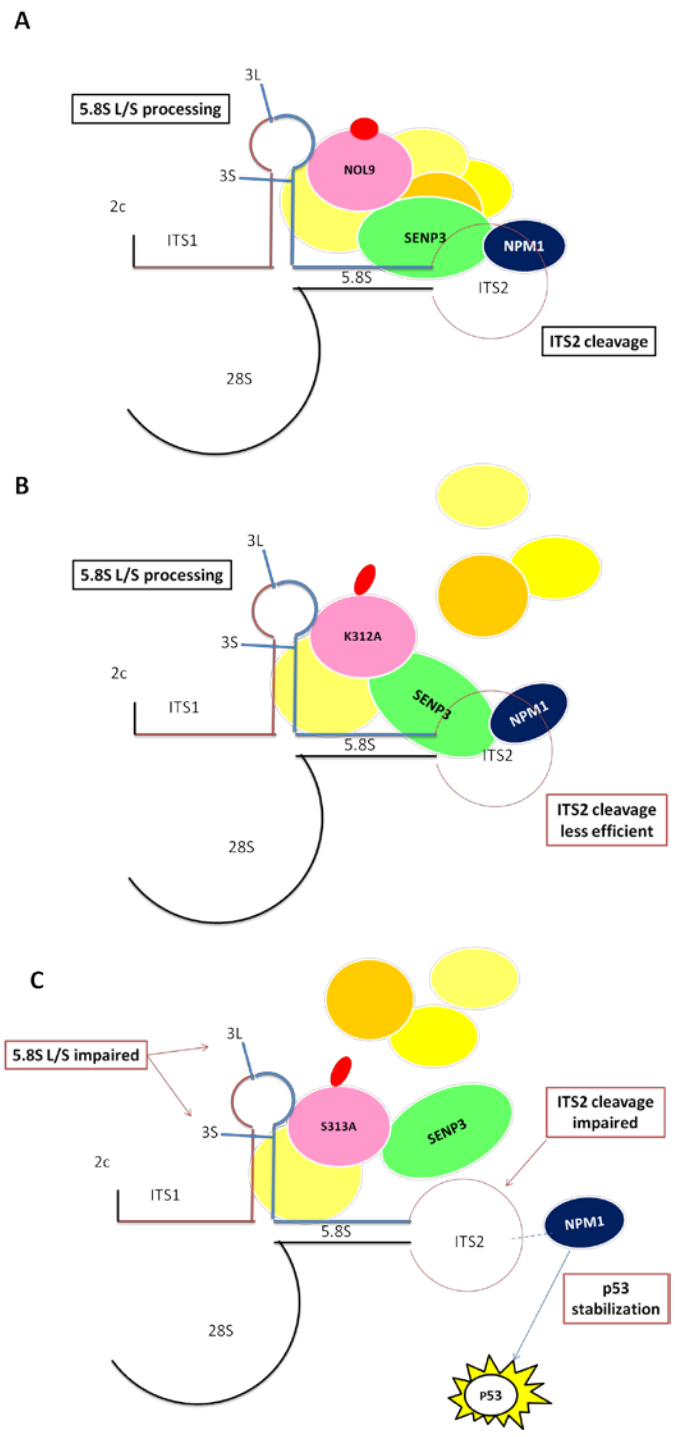

The ability of NOL9 to bind ATP is important to maintain the ITS2 complex integrity and therefore coordinate the processing at the 5' end of the 5.8S and the cleavage within ITS2. The red circle indicates ATP in association with NOL9.

MATERIALS AND METHODS

Cell culture, knockdown and transfections

HeLa cells were cultured as described in Weitzer & Martinez, 2007). SiRNA-directed knockdown was performed using Lipofectamine 2000 reagent (Invitrogen) (Heindl & Martinez, 2010) using the following siRNAs:

- siRNA Smart Pool, human NOL9 (Dharmacon, L-019418-02)
- siRNA Smart Pool, mouse Nol9 (Dharmacon, L-049328-01)
- siRNA Smart Pool, human POP1 (Dharmacon, L-014148-02)
- siRNA Smart Pool, human XRN2(Dharmacon, L-017622-01)
- siRNA Smart Pool, human NOL12 (Dharmacon, L-014330-02)
- siRNA Smart Pool, human TEX10 (Dharmacon, M-020741-01)
- siRNA Smart Pool, human SENP3 (Dharmacon, M-006034-01)
- siRNA Smart Pool, human PELP1 (Dharmacon, M-004463-01)
- siRNA Smart Pool, human WDR18 (Dharmacon, M-021451-01)

Knock down efficiency was determined by qRT-PCR using standard conditions and QIAGEN QuntiTect Primer Assays using the following primers:

- NOL9F CAGACCAGCTCTTGGGAAAG
- NOL9R GAGGACAGAGTCGGAAGCAC
- XRN2F AGTGAACCTGAGCCAGAGGA
- XRN2RTGCAATGCCTTCAAAGTCTG
- RNAMRPf TGCTGAAGGCCTGTATCCT
- RNAMRPr TGAGAATGAGCCCCGTGT
- POP1F GAGGCCAGTGAAAACCATGT
- POP1R GCAAGCCTCTCTGGTCAATC
- PELP1F AGCAGCACTGTGTGTCTTGG
- PELP1R TTCCAATGCTGACTGCTCAC
- WDR18F ACCAGACGGTGAAGCTATGG
- WDR18R GTGGAAGCTCCTCTCCCTCT
- TEX10F TTGCAACTTGCTCATCTTGG
- TEX10R AGAGTCTGCAGGGAGAACCA
- SENP3F TTTTGATGCCTCAGCAAGTG
- SENP3R ATGTCAGCGAGGTGCTTTTT
- HPRT3UTRF AGTTCTGTGGCCATCTGCTT
- HPRT3UTRR TAAACAACAATCCGCCCAAA
- mNol93f GGAGCTGAGAGCCGTATTTT

- mNol93r GCCTGCCTTCAAAAAGGTTA
- mGAPDHF ACTCCACTCACGGCAAATTC
- mGAPDHR TCTCCATGGTGGTGAAGACA

Inducible NOL9 gene deletion in MEFs

NOL9 flox/+ female mice were crossed to the Rosa26-creERT2 strain (Seibler et al. 2003). Primary MEF cells were derived from E14.5 embryos of NOL9 flox/+; CreERT2 and NOL9flox/flox; CreERT2 by using a standard procedure and grown in DMEM supplemented with 10% FBS. To delete the NOL9 gene in the MEFs, cells were synchronized in G0 by serum starvation with 2% FBS and treated with 0.5 uM 4-hydroxytamoxifen (4-OHT, sigma) for 48 h prior to serum stimulation. The NOL9 gene-deleted cells were harvested 72 h after serum stimulation.

Establishment of NOL9 knock-in MEFs

To establish the retrovirally infected NOL9flox/flox, CreERT2 MEFs, pMX-IRES-GFP empty vector, pMX-FLAG-NOL9-IRES-GFP, pMX-FLAG-NOL9(K328A)-IRES-GFP, and pMX-FLAG-NOL9(S329A)-IRES-GFP, were transfected into Plat-E cells (Morita S et al. 2000) using Fugene 6 transfection reagent (Roche). Cells were incubated for 48 hrs at 37°C with 5% CO2. NOL9flox/flox, CreERT2 MEFs were seeded at 2 × 105 cells per 6 well. The supernatants derived from these Plat-E cultures were centrifuged at 1500 rpm for 5 minutes and supplemented with 4µg/mL polybrene (Sigma). The MEFs were incubated in the virus/polybrene-containing supernatants for 8 hrs, and then 1mL of fresh medium was added. After 24 hours of infection, the cells were replated in 10 mL of fresh medium. Next day, 4-OHT was added to delete the NOL9 gene in the NOL9flox/flox; CreERT2 MEFs expressing wild type NOL9, NOL9 (K328A) or NOL9 (S329A) as described in above.

Northern blot analysis

RNA was extracted from HeLa cells and primary Mouse Embryonic Fibroblasts (MEFs) using TRIzol reagent (Invitrogen) according to the manufacturer, transferred to a positively charged nylon membrane (Hybond N+, GE Healthcare) in 20xSSC by capillary forces and UV-cross linked. Hybridization to 5' (^{32}P)-phosphorylated oligonucleotides was carried out overnight at 62 ^{o}C, followed by consecutive washing steps in 5% SDS/5xSSC, 1% SDS/1xSSC and 0.1% SDS/1xSSC. Radioactive signals were analyzed by phosphorimaging. For analysis of the 5.8S rRNA, total RNA was separated on a 8% urea polyacrylamide gel (Sequagel system, National Diagnostics) and transferred to a nylon membrane in 0.5% TBE with 300mA for 2 hours. For quantification of signal intensities in Northern Blot analyses the ImageQuant

analysis software by GE Healthcare was used. For the detection of 5.8S rRNA, 18S rRNA, 28S rRNA in human and mouse refer to (Heindl & Martinez, 2010). These additional probes were used:

- for detection of 36S and 17S rRNA in MEFs-KI cells
  - mITS1-4 (3'end) GTATCGGTATTTCGGGTGTGAGCGAACTCA
- for detection of 36S and 5'extended 5.8S in human cells
  - hITS1 (3end) GGTCGATTTGGCGAGGGCGCTCCCGACG
- for normalization in human and mouse
  - h5S GGTATTCCCAGGCGGTCTCCC.

In vitro kinase assay

RNA-phosphorylation assays were carried out as described in Weitzer & Martinez 2007, in the presence of 5mM γ-(^{32}P)-ATP and non-radio labeled scrambled ssRNA.

Retroviral constructs, gene transduction and stable cell lines

The Flag-containing Gateway cassette (Invitrogen) was introduced into the retroviral vector pBMN-IRES-IGFP. Afterward the open reading frame of human Nol9 wt and mutant (K312A and S313A) was subcloned from the pDONR-201 vectors (pDONR-201_ Nol9 wt , pDONR-201_ Nol9 K312A and Nol9 pDONR-201_ S313A) into the retroviral vector pBMN. To produce recombinant amphotropic retrovirus, vectors were transiently transfected into the packaging cell line Phoenix-GP (Gag-Pol) using a calcium-phosphate protocol. Phoenix-GP was cotransfected with an expression plasmid encoding gibbon ape leukemia virus (GALV) envelope. The medium containing the retroviral supernatant (harvested 36-48 hours after transfection of packaging cells) was added to HEK293 cells in the presence of 5 mg/ml Polybrene. Infections were repeated 2 to 3 times at intervals of 12 to 24 hours using fresh virus supernatants. Cells were sorted using fluorescence-activated cell sorting (FACS) for GFP positive cells.

Immunoprecipitation of FLAG-Nol9 wild type and kinase-dead mutant.

HEK293 cells stably expressing FLAG-Nol9, FLAG-Nol9 K312A, FLAG-Nol9 S313A were harvested on ice by scraping with culture medium. Cells were collected by centrifugation and the pellet was washed in ice cold PBS. Cells were lysated on ice in buffer P500 (500 mM NaCl, 30 mM Tris-HCl pH 7.5, 2 mM MgCl2, 5 % (w/v) glycerol, 0.1 % (w/v) Triton® X-100,0,1 mM PMSF, 4 mM β-mercaptoethanol)added of 100ug/ul RNase A (QUIAGEN Cat. No. 19101) by sonication and the extract was cleared by centrifugation (20000 X g, 4 °C, 10 min).

Tagged proteins were captured with anti-FLAG M2 affinity gel (Sigma Cat. No. A2220) equilibrated in buffer 100N (80 µL of settled beads per confluent 25x25 cm cell culture dish, 13 rpm, 4 °C, 90 min). Beads were sedimented by centrifugation and washed three times with buffer 100N (100 mM NaCl, 30 mM Tris-HCl pH 7.5, 2 mM MgCl2, 5 % (w/v) glycerol, 0.1 % (w/v) Triton® X-100, 4 mM β-mercaptoethanol, and three times with buffer P500 (500 mM NaCl, 30 mM Tris-HCl pH 7.5, 2 mM MgCl2, 5 % (w/v) glycerol, 0.1 % (w/v) Triton®X-100, 0,1 mM PMSF, 4 mM β-mercaptoethanol). Elution was carried out under native conditions by competition with 3X FLAG peptide (Catalog Number F4799, prepared in 0.5 M Tris HCl, pH 7.5, with 1 M NaCl at a concentration of 25 µg/µl and diluted 5-fold with water to prepare a 3X FLAG stock solution containing 5 µg/µl of 3X FLAG peptide). For mass spectrometric analysis of proteins immunoprecipitation was carried out using low stringency buffer 100N (used for cell lysis, and all washing steps) to allow detection of weak interaction. The proteins eluted by competition with 3X FLAG peptide were separated in SDS-PAGE and selected bands were analyzed after protein reduction (DTT), alkylation (iodoacetamide) and digestion (trypsin). The peptides were resolved by nano-HPLC and analyzed on an LTQ ion trap mass spectrometer. The analysis of the data was performed using the MASCOT software (Matrix Science).

Co-immunoprecipitation, immunoblotting, and antibodies

The proteins eluted from the FLAG-IP were separated by SDS–PAGE and transferred to a nitrocellulose membrane (Immobilon-P millipore). The following antibodies were used: Nol9 antiserum 1687 was produced by Gramsch Laboratories, Germany (Heindl & Martinez, 2010), LAS1L (Sigma-Aldrich), PELP1 (Bethyl Laboratories, Montgomery, TX), NPM1 (Sigma-Aldrich), TEX10 and WDR18 (ProteinTech), SENP3 (Santa Cruz Biotechnology), p21 (BD Bioscience) p53(Cell Signaling), TSEN34 antiserum was produced by Gramsch Laboratories, Germany peptide AKKQKLEQASGASSSQEAGS, β-actin (Santa Cruz Biotechnology). Protein extracts where prepared to test the knock down efficiency using lysis buffer (30mM pH 7.4HEPES-KOH, 100mM KCL, 5mM $MgCl_2$, 10% glycerol, 0.1% NP-40, 1mM DTT, 0.1mM AEBSF).

PAR-CLIP (Photo-activatable Ribonucleoside Cross-Link and Immuno-Precipitation)

Two 50x50cm squared culture plates of HEK293 cells, stably expressing FLAG-Nol9 wildtype, were incubated for 14 hours with 100 µM 4-thiouridine (Sigma) added to the cell medium. The dry monolayer of cell was irradiated with 0.15 J/cm2 total energy of 365 nm UV light after one wash in ice-cold PBS. Cells were then collected in PBS and the pellet dissolved in 200P-P buffer (200 mM NaCl, 30 mM Tris-Cl pH7.5, 5% glycerol, 0.1% Triton X-100, 2 mM EDTA, 4 mM beta-MeOH, 1 mM NaF, 0.1mM PMSF) and sonicated (20-40% power, 50 % duty, 10 strokes). The lysate was cleared by centrifugation (14000 rpm for 30 min) and then filtered through a 5 µm membrane syringe filter (PALL acrodisc). A preliminary RNase treatment was performed at this stage by adding RNase T1 (Fermentas) to the cleared lysate at a

final concentration of 1 U/µl and incubated in a water bath for 15 min at 22 ^{o}C. The reaction was quenched by addition of NaCl to a final concentration of 500 mM NaCl. FLAG-Nol9 was affinity purified using FLAG M2 beads suspension (Sigma), which has been equilibrated with 500P buffer (500 mM NaCl, 30 mM Tris-Cl pH7.5, 5% glycerol, 0.1% Triton X-100, 2 mM EDTA, 4 mM beta-MeOH, 1 mM NaF, 0.1mM PMSF). Beads were then washed 4 times with 500P buffer and 3 times with 300N buffer (300 mM NaCl, 30 mM Tris-Cl pH7.5, 5% glycerol, 0.1% Triton X-100, 4 mM beta-MeOH). RNase treatment was repeated using 100 U/µl of RNase T1 for 15 min at 22 ^{o}C . After 3 washes with 300N bufferthe beads were resuspended in dephosphorylation buffer (50 mM Tris-Cl pH 7.9, 100 mM NaCl, 10 mM MgCl2, 1 mM DTT) and incubated with 0.5 U/µl of Calf intestinal Phosphatase (Roche) for 10 minutes at 37 C . Thus beads were first washed in phosphatase wash buffer (50 mM Tris-Cl pH7.5, 20 mM EGTA-NaOH pH 7.5, 0.5% NP40) and then with PNK buffer without DTT (50 mM Tris-Cl pH7.5, 50 mM NaCl, 10 mM MgCl2). T4 PNK (NEB) treatment was performed after resuspension of beads in 1x bed volume of PNK buffer with DTT (50 mM Tris-Cl pH7.5, 50 mM NaCl, 10 mM MgCl2, 5 mM DTT) upon addition of γ-32P-ATP to a final concentration of 0.1 µCi/µl and T4 PNK (NEB) to 1 U/µl for 30 min at 37 ^{o}C .To quench the reaction 100 µM non-radioactive ATP was added followed by further 5 min incubation at 37 ^{o}C and 5 washes with 800 µl of PNK buffer without DTT. Radiolabeled and crosslinked RNA-Protein complexes resuspended in SDS-PAGE loading buffer and boiled were separated by SDS-PAGE (NuPAGE® 4-12% Bis-Tris Gel, Invitrogen). Bands corresponding to the expected size of the proteins of interest were detected by autoradiography, cut out and eluted in 200 µl SDS-PAGE elution buffer (20 mM Tris pH 6.8, 0.1 mM EDTA. 0.3 M NaCl, 0.1 % SDS). The gel slice homogenate was filtered through micropore filter (Ultrafree-MC, 0.22mm, Millipore) and Proteinase K treatment was performed using Proteinase K Buffer (100 mM Tris-Cl pH7.5, 12.5 mM EDTA, 150 mM NaCl, 2% SDS), followed by the addition of Proteinase K (Roche) to a final concentration of 1.2 mg/ml. Incubate for 30 min at 55 ^{o} C. Phenol/ chloroform extraction of RNA was followed by adaptor ligation for high-throughput sequencing; the RNA was ligated overnight on ice to 3’ adapter oligonucleotides (5’- App-UCG UAU GCC GUC UUC UGC UUG UidT-3’) using T4 RNA ligase 2 (truncated, NEB) including 15% polyethylene glycol 8000. The radioactively labeled RNA ligated to the 3’ adapter was separated by a preparative 15% denaturing polyacrylamide gel, excised and passively eluted and ethanol precipitated. 5’ adapter oligonucleotides (5’-GUU CAG AGU UCU ACA GUC CGA CGA UC-3’) were ligated to the RNA using T4 RNA ligase I (NEB) including 15 % polyethylene glycol 8000 on ice overnight. RNA was again separated on a 12% denaturing polyacrylamide gel and eluted from the gel region containing the radioactively labeled RNA. For cDNA preparation, Illumina Rev primer (5’-CAA GCA GAA GAC GGC ATA CGA-3’) and Superscript II Reverse Transcriptase kit (Invitrogen) was used. PCR amplification was performed using Phusion High Fidelity Polymerase (NEB) and Illumina Forward (5’- AAT GAT ACG GCG ACC ACC GAC AGG TTC AGA GTT CTA CAG TCC GA-3’) and Reverse primers. PCR products were subsequently sequenced on an Illumina G2 platform.

Immunofluorescence

Cells grown on coverslips were fixed with 3% paraformaldehyde at room temperature for 1 hr. Cells were then permeabilized with 0.3% Triton for 5 min on ice. All samples were blocked with 3% bovine

serum albumin (BSA) for 30 min, washed with PBS, and incubated with anti FLAG antibody (SIGMA ALDRICH) for 2 h at 37 °C. Cells were washed with 0,1% BSA containing 0.1% Tween-20 and incubated with secondary antibody for 1 h (Alexa Fluor 568 donkey anti–mouse antibody; Invitrogen). Cells were washed again with BSA containing 0.1% Tween-20, and mounted on slides with Vectashield (Vector Laboratories, Burlingame, CA).

Transcriptional Run On and Slot Blot analysis

Nol9 knockout primary MEFs were collected by centrifugation (1000 rpm, 3 min) after trypsinization. P53-/- MEFs were transfected with scrambled siRNA or siRNA against mouse NOL9 for 6 days (2 x 10 cm plate each) and collected as well by centrifugation (1000 rpm, 3 min) after trypsinization. The pellet was washed in cold PBS twice. Nuclei were isolated in buffer D (10mM Tris-HCl pH 7.5, 10 mM NaCl, 2.5 mM $MgCl_2$, 40 ug/ml digitonin) after 10 min of incubation on ice and collected by centrifugation (500g, 5 min, 4 °C). The collected nuclei were then resuspended in buffer E (50 mM Tris-HCl pH 7.5, 5 mM $MgCl_2$, 150mM NaCl, 25% glycerol, 1mM DTT, 6mM NaF, 0.1 mM AEBSF, 25 u/ml RNase Inhibitor by Promega) containing ATP, GTP, CTP and α^{32}P-UTP (0. 5 mM each). In nuclei transcription was performed at 30 °C for 15 min, followed by RNA isolation according to the TRIzol protocol. DNAse RQ1 (Promega) treatment of isolated RNA was performed prior to add the RNA to the pre-hybridization solution (5x SSC, 50% formammide, 1% SDS, 100 ug/ml salmon sperm DNA denatured). For the Slot Blot analysis Hybond-NX membrane (Amersham Biosciences) was used. 5ug of DNA was loaded on the membrane by Slot Blot. DNA probes covering the termination region and the 3ETS were diluted in 6X SSC. The DNA on the membrane was incubated for 10 min in denaturing solution (1.5M NaCl, 0.5M NaOH), and neutralized for 5 min in 1M NaCl, 0.5M Tris-HCl; the membrane was then UV-crosslinked and baked. Pre-hybridization and hybridization were performed at 42 °C for 1h and 48h respectively. Washes of the membrane were performed for 20 min in 2xSSC, 0.1% SDS and for 5 min 0.2% SSC, 0.1% SDS at 42 °C. The following ssDNA probes were used:

- 28S

ACAAACCCTTGTGTCGAGGGCTGACTTTCAATAGATCGCAGCGAGGGAGCTGCTCTGCTACGTACGAAACCCCGC CCAGAAGCAGGTCGTCTACGAATGGTTTAGCGCCAGGTTCCACA

- 3ETS1

ACAAACCCTTGTGTCGAGGGCCCCGTGACGCCCGGGCGGCGACACGGTCGCGTGCGAGCGAGCGGGCGTGCGAC GGGAAAGGGCAACCGCGCGGGGGCCGAGGCGACCGC

- 3ETS2

ATCCCCCCCCCAACCACCACACGGTCGTTCGGGCAACCGCGCGGGGGCCGAGGCGACCGCAGGAGAGCGACGGA AGGGGAAAGAGAAACGAACCGTCCTCGGGAGACGGAGGAGAAGACG

- 3ETS3

AGGAGAGCGACGGAAGGGGAGGGCTGCGGCGGCAGGCGACGGCAGGCCGCGGTCGCGACGGCACGAGGCTCC
CACACCCACCTCCTCCGCCCTCCGGCTTGGCCAAGGCCGGAGGGCAAG

- 3ETS4

TCGCCGCCGCCGCCGATCCCCCTCCTCCGCCCTCCGGCTTCGGCCGTCCCCGACGGACGCGCCGAGGATGGGGAT
CCCACCGTGCGTCACCGCGCCGCGGACCCCTCCCGCCCCTCCAAC

- 3ETS5

CGCCAGAGGCCTGGCGCCGAACGCGGCGTTCACGGGAAAAACCCCTCCCGCCCCTCCAACGGCGCGCGAAGAGG
AGGGGCGGGAGTGGGGATGCTCGGGCGGAGAGAGCGCCCCCCCGGC

- 3ETS6-T1

GGCGCGCGAAGAGGAGGGGCGCCGGACCCTCTCCGCCTCCACACCGCGACATCCTCCCCTCGTACGCACGTCGCC
GCCGCACCTCCGAAGTTGGGGGGGAAAAAATGGAAGAGGCGCCGC

- T1-T2

GTCGCCCGGAGTACTGGTCGACCTCCGAAGTTGGGGGGGAGGGGACACTTTCGGACATCTGGTCGACCTCCAGC
ATCGGGGGAAAAAAAAAAAACAAAGTCGCCGGGGGGGGGGGGGGGG

- T2

GGGGACACTTTCGGACATCTGGTCGACCTCCAGCATCGGGGGAAAAAAAAAAAACAAAGTAAAAAAAAAAAAAA
GAGTCCAGAGTGGCCCCGCCGCTCCGCGCCGGGGGGGGGGGGGGGG

- T3

AAAAAAAAAAAAAAGAGTCCAGAGTGGCCCCGCCGCTCCGCGCCGGGGGGGGGGGGGGGGAAGGAGTAAAAG
ACGGACAACTGGTCGACCTAAAGGTTCCAGGAATTTAAAAAAAAAAAA

- GFP

TCACCTTCAAACTTGACTTCAGCACGTGTCTTGTAGTTCCCGTCATCTTTGAAAAATATAGTTCTTTCCTTTTGTGTCC
AAGAATGTTTCCATCTTCTTTAAAATCAATACCTTTTAACTCGATTCTATTAACAAGGGTA

In vitro RNA UV-crosslink

Affinity-purified FLAG-Nol9 and the mutants FLAG-S313A and FLAG-K312A were analyzed for the ability to bind RNA *in vitro* using T7 transcribed template covering the full sequence of the human 5.8S rRNA. *In vitro* transcription was performed using MEGAscript high yield transcription kit (Ambion) according to manufacturer instructions in the presence of 4-thio-Uridine and α-P^{32}-GTP. The template for T7 transcription was produced by PCR amplification using the primers 58S_rev GACGCTCAGACAGGCGTAG T758S_fw TAATACGACTCACTATAGGGGACTCTTAGCGGTGGATCACTC. The gel-purified radio labeled T7 transcript (200nM-1µM) was boiled and renatured at room temperature and added to 5µL of affinity purified eluate and 10X buffer (400mM KCl, 22.9mM $MgCl_2$, 50mM DTT, 10mM ATP, 0.3 unit/ µl RNaseinhibitor (Promega). The reaction was pre-incubated 15minutes at 30 C^o followed by UV-

crosslinking at 356nm on ice for 10 min. The sample was boiled in 5X SDS loading buffer and analyzed by SDS-PAGE and autoradiography.

Primer extension analyses

A total of 1 mg RNA from wildtype or Nol9 knockdown cells was used. The sequence of the primer used for the analysis is the sequent: NB82 CTAGCTGCGTTCTTCATCGACG (Heindl and Martinez 2010).

DISCUSSION

The pioneer characterization of NOL9 and its ATP-binding domain (Heindl and Martinez, 2010) opened many questions regarding the roles of an RNA kinase in ribosomal RNA processing. In this thesis I investigated the requirement of a fully active enzyme for the efficient conversion of the 32S pre-rRNA into the mature 5.8S and 28S rRNAs. I studied the contribution of a functional Walker A domain to the role of NOL9 in several aspects, exploring its function in specific steps of rRNA processing and investigating the importance of proper ATP-binding for protein-protein interactions within the complex. I analyzed in further detail the complex and the almost unexplored biogenesis of the 5.8S forms in human with a particular attention in validating the role of conserved enzymes such as RNase MRP and XRN2, revealing that this pathway is only partially conserved between yeast and human. I revealed that although in human cells, RNase MRP and XRN2 cleave and trim, respectively, the ITS1 spacer very much as in yeast, this processing step seems to be uncoupled from the biogenesis of the 5.8S rRNA. The formation of the mature 5' end of the 5.8S is surprisingly linked to the processing of a novel proximal cleavage site, located 18-23nt upstream of the 3L site. This processing step requires the presence of NOL9, however it is still unclear the exact role that the kinase plays in this step.

The biogenesis of the 5.8S rRNA.

In yeast the major form of the 5.8S rRNA, $5.8S_S$ is generated by exonuclease digestion from the cleavage site A3, which is the target for cleavage by RNase MRP. Processing from site A3 extends to the mature 5' end of $5.8S_S$ and involves different exonucleases acting in parallel pathways: the Rat1/Rai1 heterodimer (Schmitt and Clayton, 1993; Henry *et al*, 1994) and Rrp17 (Oeffinger *et al*, 2009). Formation of the 5' end of the less abundant $5.8S_L$ form requires neither RNase MRP, Rat1/Rai1 nor Rrp17 and it is believed to involve a still unidentified endonuclease that cleaves directly the mature end of $5.8S_L$ (Faber *et al*, 2006). These two alternative pathways should communicate to ensure a constant overall amount of 5.8S rRNA; depletion of RNase MRP in yeast causes a change in the distribution of 5.8S rRNA in favor of the long form. In addition, an aberrant rRNA precursor that stretches from the A2 site to the mature 3'end of the 5.8S accumulates upon depletion of RNase MRP, apparently resulting from failure to cleave within the A2-B1 region containing the MRP cleavage site A3 (Schmitt and Clayton, 1993)(Figure 7)). In MRP-depleted HeLa cells I detected the accumulation of a ~650nt-long processing intermediate, spanning from the cleavage site 2b to the cleavage site 4a (Figure 8D). This fragment is a normal intermediate of the ITS1 processing that accumulates probably as a consequence of a defective cleavage at site 2c, the equivalent cleavage site to the yeast A3, known to be the target of RNase MRP. The involvement of RNase MRP in the processing of the ITS1 is therefore conserved between yeast and human. I also report the accumulation of an aberrant product spanning from site 2c to site 3L upon depletion of XRN2 suggesting a main contribution of XRN2 in trimming the products of earlier cleavage events at the ITS1 region (Figure 9D). On the other hand it is interesting to note that the ratio of the 5.8S long and short forms is not affected upon depletion of RNase MRP although the processing at the ITS1 site 2c is (Figure

87C and 8D). At the same time replacing the endogenous Nol9 with the mutant S313A-NOL9 in primary MEFs leads to a consistent alteration of the 5.8S L/S ratio, although the trimming at the 5' end of the 32S-2c occurs efficiently (the accumulation of the 32S-2c precursors is not detected upon Nol9 Knockout) (Figure 10). These results suggest that processing at site 2c in mammals doesn't directly correlate with the 5' end maturation of the 5.8SrRNA, and thus the cleavage site that constitutes the entry point for the biogenesis of the 5' end of $5.8S_s$ might be a different one. In fact, I revealed that the formation of the mature 5' end of the 5.8S is linked to the processing of a proximal cleavage site (Figure 11) located 18-23nt upstream the 3L site (Heindl and Martinez, unpublished); based on this observation the fragment accumulated in the absence of XRN2 might correspond to the 2c-(*) site rather than 2c-3L; the distance between (*) and 3L is ~20nt and the 2c site is not exactly mapped on the human sequence, thus it is hard to accurately define the 3'-extension of this aberrant product (Figure 11). The proximal cleavage site is not used in the absence of NOL9, providing a possible explanation for the defective biogenesis of the $5.8S_S$ in that context. An equivalent endonucleolytic cleavage site in ITS1, at the base of the stem that lies 5' to the B1L site, was reported also in yeast and the product of this cleavage was detectable in Rat1/Xrn1 depleted cells as well as Rrp17 depleted cells (Oeffinger, 2009). I do not have evidences for the direct involvement of XRN2 in the processing at the proximal cleavage site but a detailed analysis of the sequence spanning from the 2c and the (*) site revealed a stretch of 18 guanosines (G-18) located 65nt upstream the site 3L (Figure 12). This is a typical sequence element that interferes with the trimming by the exonucleases of the family Rat1/Xrn1 (like XRN2) as reported by Poole and Stevens in 1995. This observation allows me to speculate that a slow processing by XRN2 downstream of the site 2c would allow the competition between the still elusive endonuclease cleaving at the 3L site and the "one that should cleave" in the (*) sites on the 32S-2c pre-rRNA (Figure 12). This competition is in favor of the endonuclease of the proximal cleavage site in normal circumstances. RNase MRP is not involved in this processing but NOL9 and XRN2 affect the ratio between the two isoforms of the 5.8S rRNA with opposite tendencies. NOL9 seems to act in favor of the endonuclease of the major pathway while the presence of XRN2 seems to act in favor of cleavage at site 3L. This cleavage site is located on the loop of a conserved hairpin structure formed between the 3' end of the ITS1 and the 5' end of the 5.8S. The role of the slow processing by XRN2 at the G18 stretch may be to allow the formation of this hairpin (and therefore the 3L site) after the trimming of the first nucleotides downstream the site 2c (Figure 12). The cleavage at site (*) seems to occur independently of the presence of XRN2 but the advantage of the endonuclease of the major pathway in cleaving the (*) site is linked to the presence of NOL9. These putative endonucleases remain to be identified but the contribution of multiple exonucleases (XRN2, NOL12) can be hypothesized for a robust processing at site (*). I could demonstrate that the presence of NOL9 is linked to the cleavage at this new proximal site, but it is still unclear its precise contribution to this step. These data lead me to exclude that the role of NOL9 in this context involves its RNA kinase activity but rather the ability of NOL9 to bind ATP to allow efficient interaction with rRNA processing factors (Figure 28).

NOL9 maintains the ITS2 complex integrity and coordinates the processing at the 5' end of the 5.8S and the ITS2 cleavage sites

NOL9 was previously reported to associate with ITS2-processing factors (PELP1, LAS1L WDR18, TEX10, SENP3, IPO5, and NPM1) (Malovannaya *et al*, 2011; Castle *et al* 2011), forming a complex required for the conversion of the 32S-2c into the 5.8S and 28S rRNAs. The processing of the 32S-2c pre-rRNA consists in the trimming of the ITS1 fragment 2c-3L/3S and the cleavage within ITS2 (Figure 28). Defective cleavage of the ITS2 region is a common phenotype for the absence of NOL9 and its partners. The fact that ITS2 does not exist in Bacteria and Archea (where the 5.8S-like molecule is part of the 23S rRNA) makes the study of the ITS2 processing particularly intriguing: early in the eukaryotic lineage, the 5.8S rRNA was derived from the 5'end of an ancestral 23S rRNA-like molecule by insertion of the ITS2 region. The intra-molecular interaction of the 23S rRNA is conserved as the inter-molecular base pairing of the 5.8S rRNA with the 25/28S rRNA via two regions of extended and conserved interaction. Also in this case the processing of pre-rRNA involves a complex combination of processing factors and structural rearrangements. In yeast, the ITS2 region was reported to be refolded during pre-rRNA maturation, from a more "open-ring" conformation into a closed hairpin structure in an active process involving ribosome synthesis factors (Peculis and Greer, 1998). It was recently reported that in *S. cerevisiae* a complex of non-enzymatic processing factors called A3-cluster assembles near the 3'end of the 5.8S rRNA and induces structural reorganization of the ITS2 to ensure that the 5' end maturation of the 5.8S precedes the ITS2 cleavage (Granneman *et al*, 2011). Some of the NOL9-associated proteins can bind RNA: in this work I show that factors such as PELP1, LAS1L and probably NOL9 itself can directly interact with the 5.8S rRNA *in vivo* and *in vitro*. I also show that only a complex containing an ATP-binding competent NOL9 can interact with the ITS2-binding factor NPM1. Thus, it is very tempting to speculate that the role of ATP-bound NOL9 in 32S-2c processing consists in coordinating the interaction between 5.8S- and ITS2-binding factors to regulate the timing of the 5'end processing of the 5.8S rRNA and the cleavage within the ITS2. Further evidences should be provided to support this hypothesis. It is also worth to note that the yeast NOL9/Grc3-containing complex is involved in heterochromatin formation in *S. pombe* (Kitano *et al*, 2011), a pathway that requires the degradation of structured transcripts. This suggests that NOL9/Grc3 and its partners may target transcripts with a rigid secondary structure and facilitate their processing and degradation. Supporting this speculation I report that the involvement of the ATP-binding domain in protein-protein interaction was already reported before for CLP1, a protein closely related to NOL9 (Ghazy, 2011; Weitzer and Martinez, 2013). To date, the exact biological relevance of the role of NOL9, especially in terms of human pathologies, remains unclear. The effect of the weak K312A-NOL9 mutation can be tolerated by the p53 surveillance pathway leading to a balanced but less efficient production of 5.8S and 28S rRNAs. On the other hand, the severe inactivation of NOL9 (as in the S313A mutant) arrests the production of the rRNA components of the large ribosome subunits, activating the p53 surveillance pathway. This is a common feature of several rRNA processing factors and ribosomal proteins and this kind of defects is reported in many bone marrow failure syndromes (i.e. Diamond-Blackfan anemia, dyskeratosis congenita, Shwachman-Bodian-Diamond syndrome (Burwick *et al*, 2012). Mutations in the RNase MRP associate with a recessively inherited developmental disorder defined as Cartilage-Hair Hypoplasia (CHH) (Mattijssen et al, 2010); this

association is often linked to the role of the yeast RNase MRP in rRNA processing and its conserved nucleolar localization in vertebrates. Here I report that although RNase MRP is involved in ITS1 processing, it is actually not essential for the production of mature rRNA. Therefore I exclude that diseases associated to mutations in MRP can be classified as ribosomopaties. Rather, I connect the disease to the other essential functions of this enzyme, i.e. cleavage of cyclin B2 mRNA involved in G2/M phase progression.

This investigation has the goal to define the role of NOL9 in the processing of the 32S pre-rRNA; at the beginning of this study, many efforts were invested in trying to justify the requirement of a 5'-polynucleotide kinase in the scenario of the 5' end processing of the 32S precursor, expecially considering the possible collaboration of this enzyme with the 5'→3' exonuclease XRN2. Anyway during this study several evidences led me to diverge from this initial hypothesis and suggested that actually the contribution that NOL9 provides to the biogenesis of the mature 5.8S and 28S rRNAs is not based on its kinase activity but rather to the ability of coordinating the efficient binding of ATP with conformational changes on the protein surface necessary for promoting protein-protein interactions, and therefore the integrity of the ITS2-processing complex.

CURRICULUM VITAE

PERSONAL INFORMATIONS

SABRINA BANDINI

Birth: 27/05/1985

Place of birth: Rome

E-mail: sabrina.bandini@imba.oeaw.ac.at

EDUCATION

9/07/2004 Diploma di maturità classica 100/100, *Liceo Orazio*, Rome.

From 2004 undergraduate studies in Biotechnology , Interfaculty , University of Rome *La Sapienza*

From 11/2007 to 02/2008 Experimental thesis on the " characterization of the microRNA 135 in the neuronal development" at the microRNA unit, prof. Carlo Presutti's group , Department of genetic and Molecular biology, University of Roma *La Sapienza.*

26/02/2008 Bachelor degree in Biotechnology, 110/110 cum laude, University of Rome *La Sapienza*

From 01/2008 graduate studies in Genomic Biotechnology, University of Rome *La Sapienza*

From 03/2008 Experimental thesis on the "characterization of the expression of two antisense transcripts: miR135 and the glycerate kinase" at the microRNA unit, prof. Carlo Presutti's group , Department of genetic and Molecular biology, University of Rome *La Sapienza.*

8/10/2009 Master Degree in Genomic Biotechnology, 110/110 cum laude, University of Rome *La Sapienza*

From 07/01/2010 PhD student in Javier Martinez's group at the Institute of Molecular Biotechnology of the Austrian Academy of Sciences (IMBA), Wien.

ACKNOWLEDGMENTS

I would like to express my sincere gratitude to my advisor Javier Martinez for giving me the opportunity to join his group and work on this challenging project, for the continuous support of my Ph.D study and research, for his patience, motivation, enthusiasm, optimism and friendship. His guidance supported me in all the time of research and writing of this thesis, helping me to shape the direction of this work with his careful and instructive comments.

Besides my advisor, I would like to thank the rest of my thesis committee: Kazufumi Mochizuki and Micheal Jantsch, who provided encouraging and constructive feedback and for their precious support and advice.

It would not have been possible to write this doctoral thesis without the help and support of the kind people around me: Stefan Weitzer for his constant help with protocols and techniques, but especially for his precious advices and fruitful discussions, Johannes Popow for his help with the experiments, for his patience in explaining things (also the most obvious) and his friendly support, Jennifer Jurkin and Anne F. Nielsen for making my everyday in the lab so pleasant, for teaching me so many things and helping me to enjoy Vienna, Barbara Mair for sharing with me knowledge, reagents and also for being such a nice company inside and outside the lab, Ariela Reiss for her friendship and her fresh sense of humor, Theresa Henkel for her help with the abstract translation and her kindness and finally Kathrin Heindl for sharing with me her project and her knowledge on the nucleolar biology. I would also like to thank all the member of the Martinez, Mochizucki and Brennecke labs for all the fun we have had in the last years.

My sincere thanks also go to Jutta Damman for her “maternal” friendship, her kindness and sensitivity, without her help I would have been probably lost in the Austrian bureaucracy.

I am very grateful to Toshikatsu Hanada for providing me with precious material, especially investing so much time to generate the mouse embryonic fibroblasts I used for my key experiments, Ido Tamir for his very precious help with the PAR-CLIP data analysis, Ivo Hofacker for the time he dedicated to me explaining the complexity of RNA structure and especially I would like to thank Nicholas Watkins for his precious advices and nice conversations.

I would like to acknowledge the financial, academic and technical support of the IMBA, the University of Vienna, the RNA biology doctoral program and in particular the FWF that provided the necessary financial support for this research.

A special thank goes to my dear friends Virginia, Donatella and Lilian for spending their time to listen to me and for making me feel at home although so far from my country.

Last but not the least; I would like to thank my parents Rossana and Stefano and my sister Sara for supporting me spiritually throughout my life.

Above all, I would like to thank my beloved husband Furio for being the fuel of my life, for his ability to give me strength and self-confidence when I need them the most, for being always a safe harbor in my turbulent life and most of all for his infinite love and patience.

REFERENCES

Balasenthil and Vadlamudi, (2003) Functional interactions between the estrogen receptor coactivator PELP1/MNAR and retinoblastoma protein. J Biol Chem. 278(24):22119-27.

Bertwistle *et al* (2004) Physical and functional interactions of the Arf tumor suppressor protein with nucleophosmin/B23. Mol Cell Biol. 2004 Feb;24(3):985-96

Borer et al (1989). Major nucleolar proteins shuttle between nucleus and cytoplasm. Cell. 56(3):379-90.

Bothner *et al* (2001) Defining the molecular basis of Arf and Hdm2 interactions. J Mol Biol. 314(2):263-77.

Braglia *et al* (2010). Role of the RNA/DNA kinase Grc3 in transcription termination by RNA polymerase I. EMBO reports, **11,**758-764.

Budde A, **Grummt** I.(**1999**) p53 represses ribosomal gene transcription. Oncogene. 18(4):1119-24.

Burwick et al (2012) Impaired ribosomal subunit association in Shwachman-Diamond syndrome. Blood;120(26):5143-52.

Castle *et al* (2013) Las1 interacts with Grc3 polynucleotide kinase and is required for ribosome synthesis in Saccharomyces cerevisiae. Nucleic Acids Research, 2013, Vol. 41, No. 2 1135–1150

Dai and Lu (2004). Ribosomal protein L23 activates p53 by inhibiting MDM2 function in response to ribosomal perturbation but not to translation inhibition. Mol Cell Biol. 7654-68.

De Vries *et al* (2000) Human pre-mRNA cleavage factor II(m) contains homologs of yeast proteins and bridges two other cleavage factors. EMBO J. 19(21):5895-904.

Dou *et al* (2005) Physical association and coordinate function of the H3 K4 methyltransferase MLL1 and the H4 K16 acetyltransferase MOF. Cell. 121(6):873-85.

El Hage *et al* (2008) Efficient termination of transcription by RNA polymerase I requires the 5' exonuclease Rat1 in yeast. Genes Dev. 22(8):1069-81.

Faber *et al* (2006) 5'-end formation of yeast 5.8SL rRNA is an endonucleolytic event. Biochem Biophys Res Commun. 345(2):796-802.

Finkbeiner *et al* (2011) SUMO routes ribosome maturation. Nucleus. 527-32.

Ghazy *et al* (2011) The interaction of Pcf11 and Clp1 is needed for mRNA 3'-end formation and is modulated by amino acids in the ATP-binding site. Nucleic Acids Res. 40(3):1214-25.

Gomez-Roman *et al* (2003). Direct activation of RNA polymerase III transcription by c-Myc. Nature 421(6920):290-4.

Gonugunta *et al* (2011). Regulation of rDNA transcription by proto-oncogene PELP1. PLoS One. e21095

Granneman *et al* (2011) A cluster of ribosome synthesis factors regulate pre-rRNA folding and 5.8S rRNA maturation by the Rat1 exonuclease. EMBO J. 30(19):4006-19.

Gutell *et al* (1990) A compilation of large subunit (23S-like) ribosomal RNA sequences presented in a secondary structure format. Nucleic Acids Res. 18 Suppl:2319-30.

Hadjiolova *et al* (1994) Processing of truncated mouse or human rRNA transcribed from ribosomal minigenes transfected into mouse cells. Mol Cell Biol. 14(6):4044-56.

Hafner *et al* (2010) PAR-CliP--a method to identify transcriptome-wide the binding sites of RNA binding proteins. J Vis Exp. 41).

Haindl *et al* (2008) The nucleolar SUMO-specific protease SENP3 reverses SUMO modification of nucleophosmin and is required for rRNA processing. EMBO Rep. 273-9.

Heindl and Martinez (2010). Nol9 is a novel polynucleotide 5'-kinase involved in ribosomal RNA processing. *The EMBO Journal* 1-11.

Henry (1994). The 5' end of yeast 5.8S rRNA is generated by exonucleases from an upstream cleavage site. EMBO J. 13(10):2452-63.

Hingorani *et al* (2000). Mapping the functional domains of nucleolar protein B23. J Biol Chem. 275(32):24451-7.

Itahana *et* al (2003). Tumor suppressor ARF degrades B23, a nucleolar protein involved in ribosome biogenesis and cell proliferation. Mol Cell.1151-64.

Kamijo *et al* (1997) Tumor suppression at the mouse INK4a locus mediated by the alternative reading frame product p19ARF.Cell. 91(5):649-59.

Kamijo *et al* (1998) Functional and physical interactions of the ARF tumor suppressor with p53 and Mdm2. Proc Natl Acad Sci U S A. 95(14):8292-7.

Kashiwaya *et al* (2010). Involvement of the tubulin tyrosine ligase-like family member 4 polyglutamylase in PELP1 polyglutamylation and chromatin remodeling in pancreatic cancer cells. Cancer Res. 70(10):4024-33.

Kitano *et al*. (2011). Roles of fission yeast Grc3 protein in ribosomal RNA processing and heterochromatic gene silencing. J Biol Chem. 286(17):15391-402.

Kos M.(2010) Yeast pre-rRNA processing and modification occur cotranscriptionally. Mol Cell. 37(6):809-20.

Kurki et al (2004). Nucleolar protein NPM interacts with HDM2 and protects tumor suppressor protein p53 from HDM2-mediated degradation. *Cancer Cell*. **5**; 465-475.

Lessard *et al* (2010) The ARF tumor suppressor controls ribosome biogenesis by regulating the RNA polymerase I transcription factor TTF-I. Mol Cell. 38(4):539-50.

Lindhal *et al* (2009) RNase MRP is required for entry of 35S precursor rRNA into the canonical processing pathway. RNA. (7):1407-16.

Malovannaya *et al* (2011) Analysis of the human endogenous coregulator complexome. Cell. 145(5):787-99.

Mattijssen et al, (2010) RNase MRP and disease. Wiley Interdiscip Rev RNA. (1):102-16.

Michot *et al* (1982) Sequence and secondary structure of mouse 28S rRNA 5'terminal domain. Organisation of the 5.8S-28S rRNA complex. Nucleic Acids Res. 10(17):5273-83.

Mol Cell. 415-24.

Morello (2011) The NIP7 protein is required for accurate pre-rRNA processing in human cells. Nucleic Acids Res. 39(2):648-65.

Mullineux and Lafontaine(2012). Biochimie. Mapping the cleavage sites on mammalian pre-rRNAs: where do we stand? 94(7):1521-32.

Nair *et al* (2010). Cyclin-dependent kinase-mediated phosphorylation plays a critical role in the oncogenic functions of PELP1.Cancer Res.70(18):7166-75.

Noble *et al* (2006) Structure of a nucleotide-bound Clp1-Pcf11 polyadenylation factor. Nucleic Acids Res. 2007;35(1):87-99.

Oeffinger *et al* (2009) Rrp17p is a eukaryotic exonuclease required for 5' end processing of Pre-60S ribosomal RNA. Mol Cell 36(5):768-81.

Okuwaki *et al* (2001). Function of nucleophosmin/B23, a nucleolar acidic protein, as a histone chaperone.FEBS Lett. 506(3):272-6.

Paushkin *et al* (2004) Identification of a human endonuclease complex reveals a link between tRNA splicing and pre-mRNA 3' end formation.Cell. 117(3):311-21.

Peculis and Greer (1998) The structure of the ITS2-proximal stem is required for pre-rRNA processing in yeast. RNA. 1610-22.

Peng *et al* (2003) A panoramic view of yeast noncoding RNA processing. Cell, 113, 919–933.

Poole and Stevens (1995) Comparison of features of the RNase activity of 5'-exonuclease-1 and 5'-exonuclease-2 of Saccharomyces cerevisiae.Nucleic Acids Symp Ser.,(33):79-81.

Ramirez *et al* (2008) Human RNA 5'-kinase (hClp1) can function as a tRNA splicing enzyme in vivo. RNA. 1737-45. doi: 10.1261/rna.1142908.

Savkur and Olson (1998). Preferential cleavage in pre-ribosomal RNA by protein B23 endoribonuclease.Nucleic Acids Res. 4508-15.

Schmitt and Clayton (1993) Nuclear RNase MRP is required for correct processing of pre-5.8S rRNA in Saccharomyces cerevisiae. Mol Cell Biol.7935-41.

Sherr *et al* (2006) p53-Dependent and -independent functions of the Arf tumor suppressor. Cold Spring Harb Symp Quant Biol. 70:129-37.

Sloan *et al* (2013) Both endonucleolytic and exonucleolytic cleavage mediate ITS1 removal during human ribosomal RNA processing. J Cell Biol. 200(5):577-88.

Sugimoto *et al* (2003) Nucleolar Arf tumor suppressor inhibits ribosomal RNA processing.

Vadlamudi *et al* (2001).Molecular cloning and characterization of PELP1, a novel human coregulator of estrogen receptor alpha. J Biol Chem. 276(41):38272-9.

Vadlamudi *et al* (2004). Deregulation of estrogen receptor coactivator proline-, glutamic acid-, and leucine-rich protein-1/modulator of nongenomic activity of estrogen receptor in human endometrial tumors. J Clin Endocrinol Metab. 89(12):6130-8.

Van Riggelen *et al* (2010). MYC as a regulator of ribosome biogenesis and protein synthesis. Nat Rev Cancer. 10(4):301-9. Review.

Venema J, **Tollervey** D. (**1999**). Ribosome synthesis in Saccharomyces cerevisiae. Annu Rev Genet.;33:261-311. Review.

Wang *et al* (2002) Wang Mutational analysis defines the 5′ kinase and 3′ phosphatase active sites of T4 polynucleotide kinase. Nucleic Acids Res. 30:1073–1080.

Weitzer and Martinez (2007). The human RNA kinase hClp1 is active on 3' transfer RNA exons and short interefering RNAs. Nature **447**: 222-226.

Weitzer and Martinez (2013). CLP1 links tRNA metabolism to progressive motor-neuron loss. Nature. 2013 495(7442):474-80.

Yeh L-CC, Lee JC (1990) Structural analysis of the internal transcribed spacer 2 of the precursor ribosomal RNA from Saccharomyces cerevisiae. J Mol Biol 211:699–712.

Yun *et al* (2008). Nucleolar protein B23/nucleophosmin regulates the vertebrate SUMO pathway through SENP3 and SENP5 proteases. J Cell Biol. 183(4):589-95.

Zakrzewska-Placzek *et al* (2010). Arabidopsis thaliana XRN2 is required for primary cleavage in the pre-ribosomal RNA. Nucleic Acids Res. 4487-502.

Zhang Y, **Lu** (2009). H. Signaling to p53: ribosomal proteins find their way. Cancer Cell. 16(5):369-77. Review.

Zhu *et al* (2009) Ribosomal protein S7 is both a regulator and a substrate of MDM2. Mol Cell. 35(3):316-26.